

Article

A Responsible Machine Learning Workflow

With Focus on Interpretable Models, Post-hoc Explanation, and Discrimination Testing

Navdeep Gill ^{1,†}, Patrick Hall ^{1,3,†,*}, Kim Montgomery ^{1,†}, and Nicholas Schmidt ^{2,†}

¹ H2O.ai

² BLDS, LLC

³ George Washington University

* Correspondence: phall@h2o.ai; nschmidt@bldslc.com

† All authors contributed equally to this work.

Version February 4, 2020 submitted to Information

Abstract: This manuscript outlines a viable approach for training and evaluating machine learning (ML) systems for high-stakes, human-centered, or regulated applications using common Python programming tools. The accuracy and intrinsic interpretability of two types of constrained models, monotonic gradient boosting machines (MGBM) and explainable neural networks (XNN), a deep learning architecture well-suited for structured data, are assessed on simulated data and publicly available mortgage data. For maximum transparency and the potential generation of personalized adverse action notices, the constrained models are analyzed using post-hoc explanation techniques including plots of partial dependence (PD) and individual conditional expectation (ICE) and global and local Shapley feature importance. The constrained model predictions are also tested for disparate impact (DI) and other types of discrimination using measures with long-standing legal precedents, adverse impact ratio (AIR), marginal effect (ME), standardized mean difference (SMD), and also with straightforward group fairness measures. By combining interpretable models, post-hoc explanation, and discrimination testing with accessible software tools, this text aims to provide a template workflow for important ML applications that require high accuracy and interpretability and that mitigate risks of discrimination.

Keywords: Machine Learning; Neural Network; Gradient Boosting Machine; Interpretable; Explanation; Fairness; Disparate Impact; Python

0. Introduction

Responsible artificial intelligence (AI) has been variously conceptualized as AI-based products or projects that use transparent technical mechanisms, that create appealable decisions or outcomes, that perform reliably and in a trustworthy manner over time, that exhibit minimal social discrimination, and that are designed by humans with diverse experiences, both in terms of demographics and professional backgrounds.¹ Although responsible AI is today a somewhat broad and amorphous notion, at least one aspect is becoming clear. ML models, a common application of AI, can present serious risks. ML models can be inaccurate and unappealable black-boxes, even with the application of newer post-hoc explanation techniques [1].² ML models can perpetuate and exacerbate discrimination [2], [3], [4]. ML models can be hacked, resulting in manipulated model outcomes or the exposure

¹ See: [Responsible Artificial Intelligence, Responsible AI: A Framework for Building Trust in Your AI Solutions](#), PwC's Responsible AI, Responsible AI Practices.

² See: [When a Computer Program Keeps You in Jail](#).

of proprietary intellectual property or sensitive training data [5], [6], [7], [8]. This manuscript makes no claim that these interdependent issues of opaqueness, discrimination, privacy harms, and security vulnerabilities in ML have been resolved, even as singular entities, and much less as complex intersectional phenomena. However, Sections 1, 2, and 3 do propose some specific technical countermeasures, mostly in the form interpretable models, post-hoc explanation, and DI and discrimination testing implemented in widely available Python tools, that responsible practitioners can use to address a subset of these vexing problems.^{3,4}

Section 1 describes methods and materials, including collected training datasets, interpretable and constrained models, post-hoc explanations, tests for DI and other social discrimination, and public and open source software resources associated with this text. In Section 2, interpretable and constrained modeling results are compared to less interpretable and unconstrained models, and post-hoc explanation and discrimination testing results are also presented for interpretable models. Of course, an even wider array of tools and techniques are likely helpful to fully minimize discrimination, inaccuracy, privacy, and security risks associated with ML models. Section 3 puts forward a more holistic responsible ML modeling workflow, and addresses the burgeoning Python ecosystem for responsible AI, along with appeal and override of automated decisions, and discrimination testing and remediation in practice. Section 4 closes this manuscript with a brief summary of the outlined methods, materials, results, and discussion.

1. Materials and Methods

The simulated data (see Subsection 1.1) is based on the well-known Friedman datasets. Its known feature importance and discrimination characteristics are used to gauge the validity of interpretable modeling, post-hoc explanation, and discrimination testing techniques [10], [11]. The mortgage data (see Subsection 1.2) is sourced from the Home Mortgage Disclosure Act (HMDA) database and is a fairly realistic data source for demonstrating the template workflow.⁵ To provide a sense of accuracy differences, performance of more interpretable constrained ML models and less interpretable unconstrained ML models is compared on simulated data and collected mortgage data. Because the unconstrained ML models, gradient boosting machines (GBMs) (e.g. [12], [13]) and artificial neural networks (ANNs) (e.g. [14], [15], [16], [17]), do not exhibit convincing accuracy benefits on the simulated or mortgage data and can also present unmitigated risks, further explanation and discrimination analyses are applied only to the constrained, interpretable ML models [1], [18], [19]. Here, MGBMs⁶ (See Subsection 1.3) and XNNs (see Subsection 1.4, [20] [21]) will serve as those more interpretable models for subsequent explanatory and discrimination analyses. MGBM and XNN interpretable model architectures are selected for the example workflow because they are straightforward variants of popular unconstrained ML models. If practitioners are working with GBM and ANN models, it should be relatively uncomplicated to also evaluate the constrained versions of these models.

The same can be said of the selected explanation methods and discrimination tests. Due to their post-hoc nature, they can often be shoe-horned into existing ML workflows and pipelines. Presented explanation techniques include PD and ICE (see Subsection 1.5) and Shapley values (see Subsection 1.6) [13], [22], [23], [24]. PD, ICE, and Shapley values provide direct, global, and local summaries and

³ This text and associated software are not, and should not be construed as, legal advice or requirements for regulatory compliance.

⁴ In the United States (US), interpretable models, explanations, DI testing, and the model documentation they enable may be required under the Civil Rights Acts of 1964 and 1991, the Americans with Disabilities Act, the Genetic Information Nondiscrimination Act, the Health Insurance Portability and Accountability Act, the Equal Credit Opportunity Act (ECOA), the Fair Credit Reporting Act (FCRA), the Fair Housing Act, Federal Reserve SR 11-7, and the European Union (EU) General Data Protection Regulation (GDPR) Article 22 [9].

⁵ See: [Mortgage data \(HMDA\)](#).

⁶ As implemented in [XGBoost](#) or [h2o](#).

descriptions of constrained models without resorting to the use of intermediary and approximate surrogate models. Discussed discrimination testing methods (see Subsection 1.7) include AIR, ME, and SMD [2], [25], [26].⁷ Accuracy and other confusion matrix metrics are also reported by demographic segment [27]. All outlined materials and methods are implemented in open source Python code, and are made available on GitHub (see Subsection 1.8).

1.1. Simulated Data

Simulated data is created based on a signal-generating function, f , first proposed in Friedman [10] and extended in Friedman *et al.* [11]:

$$f(\mathbf{X}) = 10 \sin(\pi \mathbf{X}_{\text{Friedman},1} \mathbf{X}_{\text{Friedman},2}) + 20(\mathbf{X}_{\text{Friedman},3} - 0.5)^2 + 10 \mathbf{X}_{\text{Friedman},4} + 5 \mathbf{X}_{\text{Friedman},5} \quad (1)$$

where $\mathbf{X}_{\text{Friedman},j}$ are random uniform features in $[0, 1]$. In Friedman's texts, a Gaussian noise term was added to create a continuous output feature for testing spline regression methodologies. In this manuscript, the signal generating function and input features are modified in several ways. Two binary features, a categorical feature with five discrete levels, and a bias term are introduced into f to add a degree of complexity that may more closely mimic real-world settings. For binary classification analysis, the Gaussian noise term is replaced with noise drawn from a logistic distribution and coefficients are re-scaled to be one fifth of the size of those used by Friedman, and any $f(\mathbf{X})$ value above 0 is classified as a positive outcome, while $f(\mathbf{X})$ values less than or equal to zero are designated as negative outcomes. Finally, f is augmented with two hypothetical protected class-control features with known dependencies on the binary outcome to allow for discrimination testing. The simulated data is generated to have eight input features, twelve after numeric encoding of categorical features, and a binary outcome, two class-control features, and 100,000 instances. The simulated data is then split into a training and test set, with 80,000 and 20,000 observations, respectively. Within the training set, a 5-fold cross-validation indicator is used for training all models. For an exact specification of the simulated data, see the software resources referenced in Subsection 1.8.

1.2. Mortgage Data

The mortgage dataset analyzed here is a random sample of consumer-anonymized loans from the HDMA database. These loans are a subset of all originated mortgage loans in the 2018 HMDA data that were chosen to represent a relatively comparable group of consumer mortgages. A selection of features is used to predict whether a loan is *high-priced*, i.e., the annual percentage rate (APR) charged was 150 basis points (1.5%) or more above a survey-based estimate of other similar loans offered around the time of the given loan. After data cleaning and preprocessing to encode categorical features and create missing markers, the mortgage data contains ten input features and the binary outcome, *high-priced*. The data is split into a training set with 160,338 loans and a marker for 5-fold cross-validation and a test set containing 39,662 loans. While lenders would almost certainly use more information than the selected features to determine whether to offer and originate a high-priced loan, the selected input features (loan to value (LTV) ratio, debt to income (DTI) ratio, property value, loan amount, introductory interest rate, customer income, etc.) are likely to be some of the most influential factors that a lender would consider. See Appendix A for general information regarding HMDA data.

1.3. Monotonic Gradient Boosting Machines

MGBMs constrain typical GBM training to consider only tree splits that obey user-defined positive and negative monotonicity constraints, with respect to each input feature, X_j , and a target feature, y ,

⁷ Part 1607 - Uniform Guidelines on Employee Selection Procedures (1978) §1607.4.

¹⁰⁸ independently. An MGBM remains an additive combination of B trees trained by gradient boosting,
¹⁰⁹ T_b , and each tree learns a set of splitting rules that respect monotonicity constraints, Θ_b^{mono} . For some
¹¹⁰ instance, \mathbf{x} , a trained MGBM model, g^{MGBM} , takes the form:

$$g^{\text{MGBM}}(\mathbf{x}) = \sum_{b=0}^{B-1} T_b(\mathbf{x}; \Theta_b^{\text{mono}}) \quad (2)$$

¹¹¹ As in unconstrained GBM, Θ_b^{mono} is selected in a greedy, additive fashion by minimizing a regularized
¹¹² loss function that considers known target labels, the predictions of all subsequently trained trees
¹¹³ in g^{MGBM} , and the b -th tree splits applied to \mathbf{x} , $T_b(\mathbf{x}^{(i)}; \Theta_b^{\text{mono}})$, in a numeric loss function (e.g.,
¹¹⁴ squared loss, Huber loss), and a regularization term that penalizes complexity in the current tree. See
¹¹⁵ Appendices B.1 and B.2 for details pertaining to MGBM training.

¹¹⁶ Herein, two g^{MGBM} models are trained. One on the simulated data and one on the mortgage
¹¹⁷ data. In both cases, positive and negative monotonic constraints for each X_j are selected using
¹¹⁸ domain knowledge, random grid search is used to determine other hyperparameters, and 5-fold
¹¹⁹ cross-validation and test partitions are used for model assessment. For exact parameterization of the
¹²⁰ two g^{MGBM} models, see the software resources referenced in Subsection 1.8.

¹²¹ 1.4. Explainable Neural Networks

¹²² XNNs are an alternative formulation of additive index models in which the ridge functions are
¹²³ neural networks [20]. XNNs also bear a strong resemblance to generalized additive models (GAMs)
¹²⁴ and so-called explainable boosting machines (EBMs or GA²M), i.e., GAMs which consider main
¹²⁵ effects and a small number of 2-way interactions and may also incorporate boosting into their training
¹²⁶ [13], [28]. Hence, XNNs enable users to tailor interpretable neural network architectures to a given
¹²⁷ prediction problem and to visualize model behavior by plotting ridge functions. A trained XNN
¹²⁸ function, g^{XNN} , applied to some instance \mathbf{x} , is defined as:

$$g^{\text{XNN}}(\mathbf{x}) = \mu_0 + \sum_{k=0}^{K-1} \gamma_k n_k \left(\sum_{j=0}^{J-1} \beta_{k,j} x_j \right) \quad (3)$$

¹²⁹ where μ_0 is a global bias for K individually specified ANN subnetworks, n_k , with scale parameters γ_k .
¹³⁰ The inputs to each n_k are themselves a linear combination of the J modeling inputs and their associated
¹³¹ $\beta_{k,j}$ coefficients in the deepest projection layer.

¹³² Two g^{XNN} models are trained by mini-batch stochastic gradient descent (SGD) on the simulated
¹³³ data and mortgage data. Each g^{XNN} is assessed in 5 training folds and in a test data partition. L_1
¹³⁴ regularization is applied to network weights to induce a sparse and interpretable model, where each
¹³⁵ n_k and corresponding γ_k are ideally associated with an important X_j or combination thereof. The g^{XNN}
¹³⁶ models appear highly sensitive to weight initialization and batch size. Be aware that g^{XNN} model
¹³⁷ architectures may require manual and judicious feature selection due to long training times. For more
¹³⁸ details regarding g^{XNN} training, see the software resources in Subsection 1.8 and Appendices B.1 and
¹³⁹ B.3.

¹⁴⁰ 1.5. One-dimensional Partial Dependence and Individual Conditional Expectation

¹⁴¹ PD plots are a widely-used method for describing and plotting the estimated average prediction
¹⁴² of a complex model, g , across some partition of data, \mathbf{X} , for some interesting input feature, X_j [13].
¹⁴³ ICE plots are a newer method that describes the local behavior of g with regard to values of an input
¹⁴⁴ feature, x_j , in a single instance, \mathbf{x} . PD and ICE can be overlaid in the same plot to create a holistic
¹⁴⁵ global and local portrait of the predictions for some g and X_j [22]. When $\text{PD}(X_j, g)$ and $\text{ICE}(x_j, g)$
¹⁴⁶ curves diverge, such plots can also be indicative of modeled interactions in g or expose flaws in PD
¹⁴⁷ estimation, e.g., inaccuracy in the presence of strong interactions and correlations [22], [29]. For details

¹⁴⁸ regarding the calculation of one-dimensional PD and ICE, see the software resources in Subsection 1.8
¹⁴⁹ and Appendices B.1 and B.4.

¹⁵⁰ 1.6. *Shapley Values*

¹⁵¹ Shapley explanations are a class of additive, locally accurate feature contribution measures with
¹⁵² long-standing theoretical support [23], [30]. Shapley explanations are the only locally accurate and
¹⁵³ globally consistent feature contribution values, meaning that Shapley explanation values for input
¹⁵⁴ features always sum to $g(\mathbf{x})$ for any \mathbf{x} , and that Shapley explanation values should not decrease
¹⁵⁵ in magnitude for some x_j when g is changed such that x_j truly makes a stronger contribution to
¹⁵⁶ $g(\mathbf{x})$ [23], [24]. Shapley values can be estimated in different ways, many of which are intractable for
¹⁵⁷ datasets with large numbers of input features. Tree SHAP (SHapley Additive exPlanations) is a specific
¹⁵⁸ implementation of Shapley explanations that relies on traversing internal decision tree structures to
¹⁵⁹ efficiently estimate the contribution of each x_j for some $g(\mathbf{x})$ [24]. Tree SHAP has been implemented
¹⁶⁰ in popular gradient boosting libraries such as `h2o`, `LightGBM`, and `XGBoost`, and Tree SHAP is used to
¹⁶¹ calculate accurate and consistent global and local feature importance for MGBM models in Subsection
¹⁶² 2.2.2 and Appendix E.1. Deep SHAP is an approximate Shapley value technique that creates SHAP
¹⁶³ values for ANNs [23]. Deep SHAP is implemented in the `shap` package and is used to generate SHAP
¹⁶⁴ values for the two g^{XNN} models discussed in Subsection 2.2.2 and Appendix E.1. For more information
¹⁶⁵ pertaining to the calculation of Shapley values, see Appendices B.1 and B.5.

¹⁶⁶ 1.7. *Discrimination Testing Measures*

¹⁶⁷ Because many technical and academic discussions of fairness in ML have been inconclusive⁸,
¹⁶⁸ this text will draw on regulatory and legal standards that have been used for years in regulated,
¹⁶⁹ high-stakes employment and financial decisions. The discussed measures are also representative of
¹⁷⁰ fair lending analyses and pair well with the mortgage data. See Appendix C for a brief discussion
¹⁷¹ regarding different types of discrimination under US laws and Appendix D for remarks on practical vs.
¹⁷² statistical significance for discrimination measures. One common measure of DI used in US litigation
¹⁷³ and regulatory settings is ME. ME is simply the difference between the percent of the control group
¹⁷⁴ members receiving a favorable outcome and the percent of the protected class members receiving a
¹⁷⁵ favorable outcome.

$$\text{ME} \equiv 100 \cdot (\Pr(\hat{\mathbf{y}} = 1 | X_c = 1) - \Pr(\hat{\mathbf{y}} = 1 | X_p = 1)) \quad (4)$$

¹⁷⁶ where X_p and X_c represent binary markers created from some demographic attribute, c denotes the
¹⁷⁷ control group (often whites or males), p indicates a protected group, and $\Pr(\cdot)$ is the operator for
¹⁷⁸ conditional probability. ME is a favored DI metric used by the US Consumer Financial Protection
¹⁷⁹ Bureau (CFPB), the primary agency charged with regulating fair lending laws at the largest US lending
¹⁸⁰ institutions and for various other participants in the consumer financial market.⁹ Another important
¹⁸¹ DI measure is AIR, more commonly known as a *relative risk ratio* in settings outside of regulatory
¹⁸² compliance.

$$\text{AIR} \equiv \frac{\Pr(\hat{\mathbf{y}} = 1 | X_p = 1)}{\Pr(\hat{\mathbf{y}} = 1 | X_c = 1)} \quad (5)$$

¹⁸³ AIR is equal to the ratio of the proportion of the protected class that receives a favorable outcome
¹⁸⁴ divided by the proportion of the control class that receives a favorable outcome. Statistically significant
¹⁸⁵ AIR values below 0.8 can be considered *prima facia* evidence of discrimination. An additional

⁸ See: [Tutorial: 21 Fairness Definitions and Their Politics](#).

⁹ See: [Supervisory Highlights, Issue 9, Fall 2015](#).

long-standing measure of DI is SMD. SMD is often used to assess disparities in continuous features, such as income differences in employment analyses, or interest rate differences in lending. It originates from work on statistical power, and is more formally known as *Cohen's d*. SMD is equal to the difference in the average protected class outcome, \bar{y}_p , minus the control class outcome, \bar{y}_c , divided by a measure of the standard deviation of the population, $\sigma_{\bar{y}}$.¹⁰ Cohen defined values of this metric to have *small*, *medium*, and *large* effect sizes if the values exceeded 0.2, 0.5, and 0.8, respectively.

$$\text{SMD} \equiv \frac{\bar{y}_p - \bar{y}_c}{\sigma_{\bar{y}}} \quad (6)$$

The numerator in the SMD is equivalent to ME but adds the standard deviation divisor as a standardizing factor. Because of this standardization factor, SMD allows for a comparison across different types of outcomes, such as inequity in mortgage closing fees or inequities in the interest rates given on certain loans. In this, one may apply definitions in Cohen [25] of *small*, *medium*, and *large* effect sizes, which represent a measure of *practical significance*, which is described in detail in Appendix D. Finally, confusion matrix measures in demographic groups, such as accuracy, false positive rate (FPR), and their ratios, are also considered as measures of DI in Subsection 2.2.3 and Appendix E.2.

1.8. Software Resources

Python code to reproduce discussed results is available at: <https://github.com/h2oai/article-information-2019>. The primary Python packages employed are: `numpy` and `pandas` for data manipulation, `h2o`, `keras`, `shap`, and `tensorflow` for modeling, explanation, and discrimination testing, and `matplotlib` for plotting.

2. Results

Results are laid out for the simulated and mortgage datasets. Accuracy is compared for unconstrained, less interpretable g^{GBM} and g^{ANN} models and constrained, more interpretable g^{MGBM} and g^{XNN} models. Then, for the g^{MGBM} and g^{XNN} models, intrinsic interpretability, post-hoc explanation, and discrimination testing results are explored.

2.1. Simulated Data Results

Fit comparisons between unconstrained and constrained models and XNN interpretability results are discussed in Subsections 2.1.1 and 2.1.2. As model training and assessment on the simulated data is a rough validation exercise meant to showcase expected results on data with known characteristics, and given that most of the techniques in the proposed workflow are already used widely or have been validated elsewhere, reporting of simulated data results in the main text will focus mostly on fit measures for the considered data and model architectures and on the more novel g^{XNN} interpretability results. The bulk of the post-hoc explanation and discrimination testing results for the simulated data are left to Appendix E.

2.1.1. Constrained vs. Unconstrained Model Fit Assessment

Table 1 presents a variety of fit measures for g^{GBM} , g^{MGBM} , g^{ANN} , and g^{XNN} on the simulated test data. g^{XNN} exhibits the best performance, but the models exhibit only a fairly small range of fit results. Interpretability and explainability benefits of the constrained models appear to come at little cost to overall model performance, or in the case of g^{ANN} and g^{XNN} , no cost at all. For the displayed

¹⁰ There are several measures of the standard deviation of the score that are typically used: 1. the standard deviation of the population, irrespective of protected class status, 2. a standard deviation calculated only over the two groups being considered in a particular calculation, or 3. a pooled standard deviation, using the standard deviations for each of the two groups with weights.

measures, g^{MGBM} performs ~2% worse than g^{GBM} . g^{XNN} performs ~0.5% better on average than g^{XNN} , and g^{XNN} actually shows slightly better fit than g^{ANN} across all fit measures except specificity. Fit measures that require a probability cutoff are taken at the best F1 threshold for each model.

Table 1. Fit measures for g^{GBM} , g^{MGBM} , g^{ANN} , and g^{XNN} on the simulated test data. Arrows indicate the direction of improvement for each measure.

Model	Accuracy ↑	AUC ↑	F1 ↑	Logloss ↓	MCC ↑	RMSE ↓	Sensitivity ↑	Specificity ↑
g^{GBM}	0.757	0.847	0.779	0.486	0.525	0.400	0.858	0.657
g^{MGBM}	0.744	0.842	0.771	0.502	0.504	0.407	0.864	0.625
g^{ANN}	0.757	0.850	0.779	0.480	0.525	0.398	0.858	0.657
g^{XNN}	0.758	0.851	0.781	0.479	0.528	0.397	0.867	0.648

2.1.2. Interpretability Results

For g^{XNN} , inherent interpretability manifests as plots of sparse γ_k output layer weights, n_k subnetwork ridge functions, and sparse β_j weights in the bottom projection layer. Figure 1 provides detailed insights into g^{XNN} . 1a displays the sparse γ_k weights of the output layer, where only n_k subnetworks with $k \in \{1, 4, 7, 8, 9\}$ are associated with large magnitude weights. The n_k subnetwork ridge functions appear in 1b as simplistic but distinctive functional forms. Color-coding between 1a and 1b visually reinforces the direct feed-forward relationship between the n_k subnetworks and the γ_k weights of the output layer.

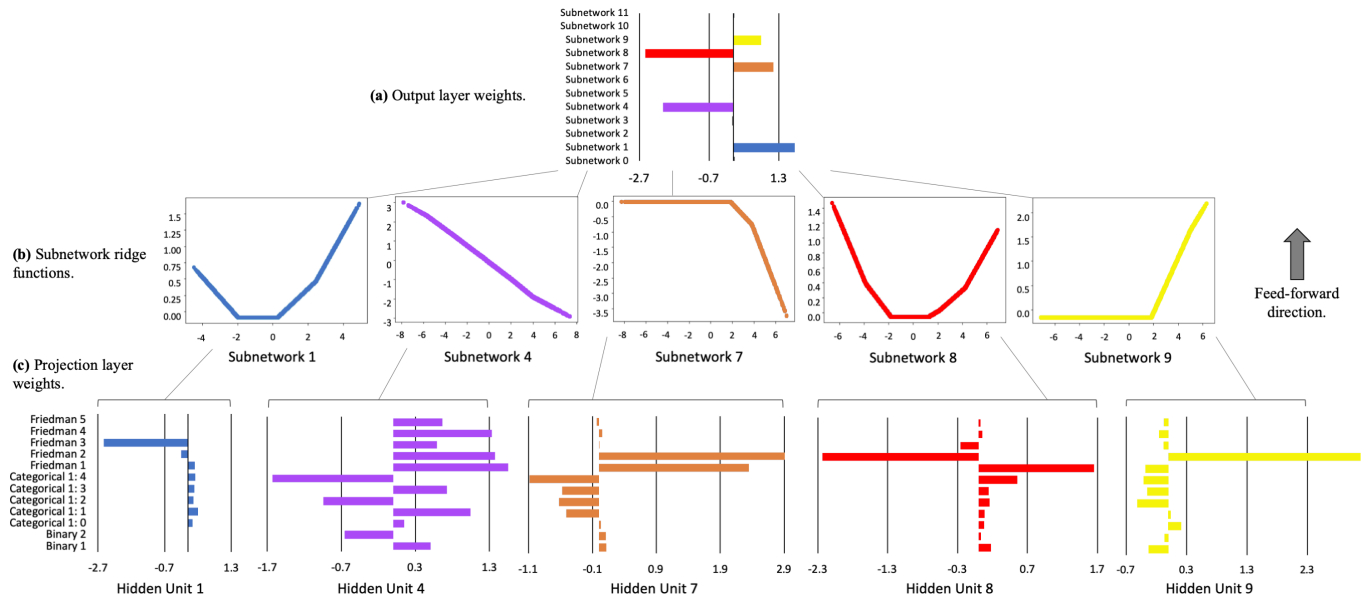


Figure 1. Output layer γ_k weights, corresponding n_k ridge functions, and associated projection layer β_j weights for g^{XNN} on the simulated test data.

n_k subnetworks are plotted across the output values of their associated $\sum_j \beta_{k,j} x_j$ projection layer hidden units, and color-coding between 1b and 1c link the β_j weights to their n_k subnetworks. Most of the heavily utilized n_k subnetworks have sparse weights in their $\sum_j \beta_{k,j} x_j$ projection layer hidden units. In particular, subnetwork n_1 appears to be almost solely a function of $X_{\text{Friedman},3}$ and appears to exhibit the expected quadratic behavior for $X_{\text{Friedman},3}$. Subnetworks n_7 , n_8 , and n_9 appear to be most associated with the globally important $X_{\text{Friedman},1}$ and $X_{\text{Friedman},2}$ features, likely betraying the effort required for g^{XNN} to model the nonlinear $\sin()$ function of the $X_{\text{Friedman},1}$ and $X_{\text{Friedman},2}$ product, and these subnetworks, especially n_7 and n_8 , appear to display some noticeable sinusoidal characteristics. Subnetwork n_4 seems to be a linear combination of all the original input X_j features, but does weigh the

linear $X_{\text{Friedman},4}$ and $X_{\text{Friedman},5}$ terms roughly in the correct two-to-one ratio. As a whole, Figure 1a, b, and c exhibit evidence that $g^{\text{XNN}}(\mathbf{X})$ has learned about the signal-generating function in Equation 1 and the displayed information should help practitioners understand which original input X_j features are weighed heavily in each n_k subnetwork, and which n_k subnetworks have a strong influence on $g^{\text{XNN}}(\mathbf{X})$ output. See Appendix B.3 for details regarding general XNN architecture.

2.2. Mortgage Data Results

Results for the mortgage data are presented in Subsections 2.2.1 – 2.2.3 to showcase the example workflow. g^{ANN} and g^{XNN} outperform g^{GBM} and g^{MGBM} on the mortgage data, but as in Subsection 2.1.1 the constrained variants of both model architectures do not show large differences in model fit with respect to unconstrained variants. Assuming that in high-stakes applications small fit differences on static test data do not outweigh the need for enhanced model debugging facilitated by high interpretability, only g^{MGBM} and g^{XNN} interpretability, post-hoc explainability, and discrimination testing results are presented.

2.2.1. Constrained vs. Unconstrained Model Fit Assessment

Table 2 shows that g^{ANN} and g^{XNN} noticeably outperform g^{GBM} and g^{MGBM} on the mortgage data for most of the fit measures. This is at least partially due to the preprocessing required to present directly comparable post-hoc explainability results and to use neural networks and tensorflow, e.g., numerical encoding of categorical features and missing values. This preprocessing appears to hamstring some of the tree-based models' inherent capabilities. g^{GBM} models trained on non-encoded data with missing values repeatedly produced area under the curve (AUC) values of ~ 0.81 (not shown, but available in resources discussed in Subsection 1.8).

Table 2. Fit measures for g^{GBM} , g^{MGBM} , g^{ANN} , and g^{XNN} on the mortgage test data. Arrows indicate the direction of improvement for each measure.

Model	Accuracy ↑	AUC ↑	F1 ↑	Logloss ↓	MCC ↑	RMSE ↓	Sensitivity ↑	Specificity ↑
g^{GBM}	0.795	0.828	0.376	0.252	0.314	0.276	0.634	0.813
g^{MGBM}	0.765	0.814	0.362	0.259	0.305	0.278	0.684	0.773
g^{ANN}	0.865	0.871	0.474	0.231	0.418	0.262	0.624	0.891
g^{XNN}	0.869	0.868	0.468	0.233	0.409	0.263	0.594	0.898

Regardless of the fit differences between the two families of models, the difference between the constrained and unconstrained variants within the two types of models is small for the GBMs and smaller for the ANNs, $\sim 3.5\%$ and $\sim 1\%$ worse fit respectively, averaged across the measures in Table 2.

2.2.2. Interpretability and Post-hoc Explanation Results

For g^{MGBM} , intrinsic interpretability is evaluated with PD and ICE plots of mostly monotonic prediction behavior for several important X_j , and post-hoc Shapley explanation analysis is used to create global and local feature importance. Global Shapley feature importance for g^{MGBM} on the mortgage test data is reported in Figure 2. g^{MGBM} places high importance on LTV ratio, perhaps too high, and also weighs DTI ratio, property value, loan amount, and introductory rate period heavily in many of its predictions. Tree SHAP values are reported in the margin space, prior to the application of the logit link function, and the reported numeric values can be interpreted as the mean absolute impact of each X_j on $g^{\text{MGBM}}(\mathbf{X})$ in the mortgage test data in the g^{MGBM} margin space. The potential over-emphasis of LTV ratio, and the de-emphasis of income, likely an important feature from a business perspective, and the encoded no introductory rate period flag feature may also contribute to the decreased performance of g^{MGBM} as compared to g^{XNN} .

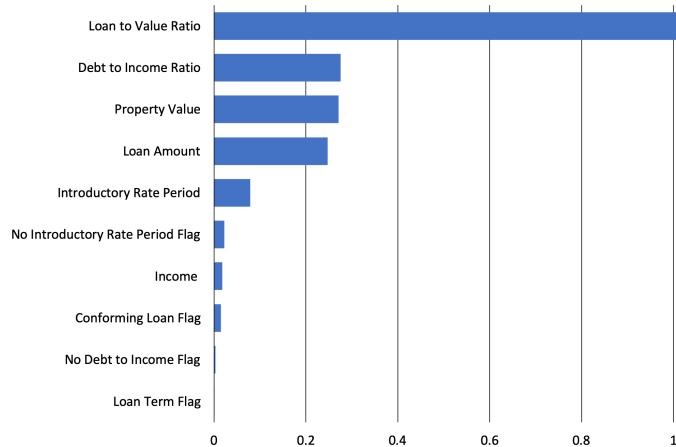


Figure 2. Global mean absolute Tree SHAP feature importance for $g^{\text{MGBM}}(\mathbf{X})$ on the mortgage test data.

279 Domain knowledge was used to positively constrain DTI ratio and LTV ratio and to negatively
 280 constrain income and the loan term flag under g^{MGBM} . The monotonicity constraints for DTI ratio
 281 and LTV ratio are confirmed for $g^{\text{MGBM}}(\mathbf{X})$ on the mortgage test data in Figure 3. Both DTI ratio
 282 and LTV ratio display positive monotonic behavior at all selected percentiles of $g^{\text{MGBM}}(\mathbf{X})$ for ICE
 283 and on average with PD. Because PD curves generally follow the patterns of the ICE curves for both
 284 features, it's also likely that no strong interactions are at play for DTI ratio and LTV ratio under
 285 g^{MGBM} . Of course, the monotonicity constraints themselves can dampen the effects of non-monotonic
 286 interactions under g^{MGBM} , even if they do exist in the data. Perhaps due to the presence of important
 287 non-monotonic interactions (e.g., LTV ratio and the no introductory rate period flag, see Figure 6).
 288 This rigidity could also play a role in the performance differences between g^{MGBM} and g^{XNN} in the
 289 mortgage data not observed for the simulated data, wherein strong interactions appear to be between
 290 features with the same monotonicity constraints (e.g., $X_{\text{Friedman},1}$ and $X_{\text{Friedman},2}$, see Figure 1).

291 PD and ICE are displayed with a histogram to highlight any sparse regions in an input feature's
 292 domain. Because most ML models will always issue a prediction on any instance with a correct
 293 schema, it's crucial to consider whether a given model learned enough about an observation to make
 294 an accurate prediction. Viewing PD and ICE along with a histogram is a convenient method to visually
 295 assess whether a prediction is reasonable and based on sufficient training data. DTI ratio and LTV
 296 ratio do appear to have sparse regions in their univariate distributions. The monotonicity constraints
 297 likely play to the advantage of g^{MGBM} in this regard, as g^{MGBM} appears to carry reasonable predictions
 298 learned from populous domains into the sparse domains of both features.

299 Figure 3 also displays PD and ICE for the unconstrained feature property value. Unlike DTI ratio
 300 and LTV ratio, PD for property value does not always follow the patterns established by ICE curves.
 301 While PD shows monotonically increasing prediction behavior on average, apparently influenced by
 302 large predictions at extreme $g^{\text{MGBM}}(\mathbf{X})$ percentiles, ICE curves for individuals at the 40th percentile
 303 of $g^{\text{MGBM}}(\mathbf{X})$, and lower, exhibit different prediction behavior with respect to property value. Some
 304 individuals at these lower percentiles display monotonically decreasing prediction behavior while
 305 others appear to show fluctuating prediction behavior. Property value is strongly right-skewed, with
 306 little data regarding high-value property from which g^{MGBM} can learn. For the most part, reasonable
 307 predictions do appear to be carried from more densely populated regions to more sparsely populated
 308 regions. However, prediction fluctuations at lower $g^{\text{MGBM}}(\mathbf{X})$ percentiles are visible, and appear in a
 309 sparse region of property value. This divergence of PD and ICE can be indicative of an interaction
 310 affecting property value under g^{MGBM} [22], and analysis by surrogate decision tree did show evidence
 311 of numerous potential interactions in lower predictions ranges of $g^{\text{MGBM}}(\mathbf{X})$ [31] (not shown, but
 312 available in resources discussed in Subsection 1.8). However, fluctuations in ICE can also be caused by

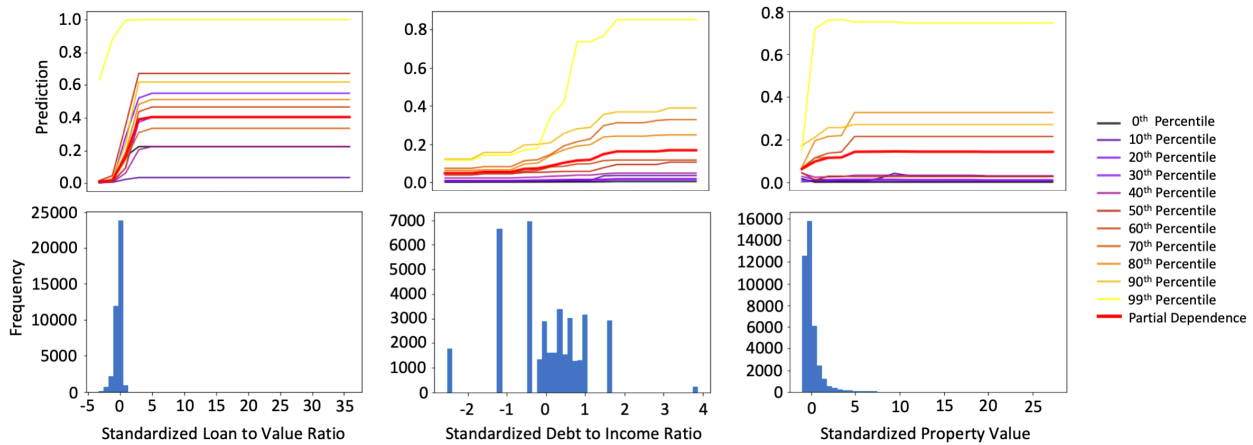


Figure 3. PD, ICE for 10 individuals across selected percentiles of $g^{\text{MGBM}}(\mathbf{X})$, and histograms for the three most important input features of g^{MGBM} on the mortgage test data.

313 overfitting or by leakage of strong non-monotonic signal from important constrained features into the
314 modeled behavior of non-constrained features.

315 In Figure 4, local Tree SHAP values are displayed for selected individuals at the 10th, 50th, and 90th
316 percentiles of $g^{\text{MGBM}}(\mathbf{X})$ in the mortgage test data. Each ϕ_j value in Figure 4 represents the difference
317 in $g^{\text{MGBM}}(\mathbf{x}^{(i)})$ and the average of $g^{\text{MGBM}}(\mathbf{X})$ associated with some input feature X_j [32]. Accordingly,
318 the logit of the sum of the Shapley values and the Shapley intercept will be the $g^{\text{MGBM}}(\mathbf{x})$ prediction in
319 the probability space, for any \mathbf{x} .

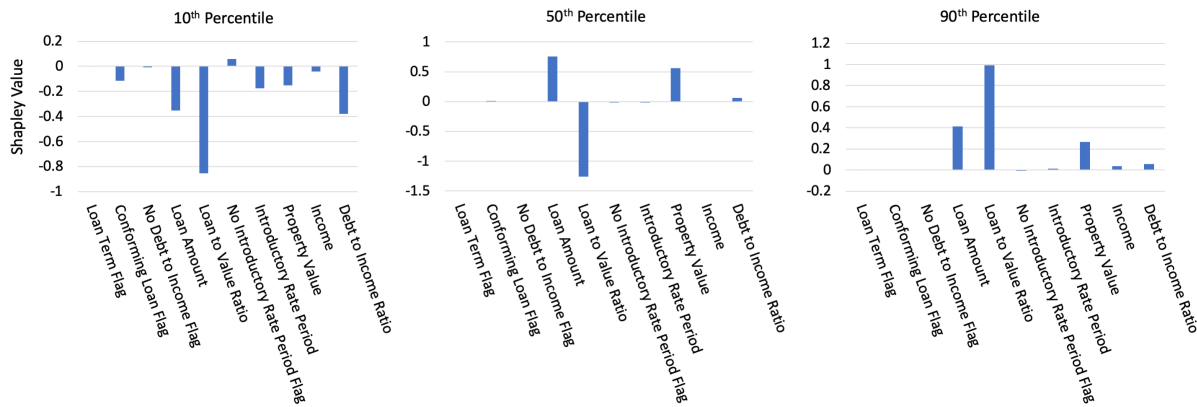


Figure 4. Tree SHAP values for three individuals across selected percentiles of $g^{\text{MGBM}}(\mathbf{X})$ for the mortgage test data.

320 The selected individuals show an expected progression of mostly negative Shapley values at the 10th
321 percentile, a mixture of positive and negative Shapley values at the 50th percentile, mostly positive
322 Shapley values the 90th percentile, and with globally important features driving most local model
323 decisions. Deeper significance for Figure 4 lies in the ability of Tree SHAP to accurately and consistently
324 summarize any single $g^{\text{MGBM}}(\mathbf{x})$ prediction in this manner, which is generally important for enabling
325 logical appeal or override of ML-based decisions, and is specifically important in the context of lending,
326 where applicable regulations often require lenders to provide consumer-specific reasons for denying
327 credit to an individual. In the US, applicable regulations are typically ECOA and FCRA, and the
328 consumer-specific reasons are commonly known as adverse actions codes.

329 Figure 5 displays global feature importance for g^{XNN} on the mortgage test data. Deep SHAP
330 values are reported in the probability space, after the application of the logit link function. They are
331 also calculated from the projection layer of g^{XNN} . Thus, the Deep SHAP values in Figure 5 are the

332 estimated average absolute impact of each X_j in the projection layer and probability space of g^{XNN} for
 333 the mortgage test data. g^{XNN} distributes importance more evenly across business drivers and puts
 334 stronger emphasis on the no introductory rate period flag feature than does g^{MGBM} . Like g^{MGBM} , g^{XNN}
 335 puts little emphasis on the other flag features.

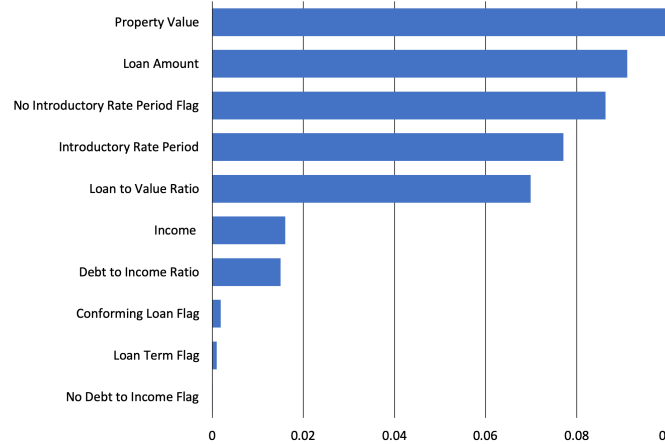


Figure 5. Global mean absolute Deep SHAP feature importance for $g^{\text{XNN}}(X)$ on the mortgage test data.

336 As compared to g^{MGBM} , g^{XNN} assigns higher importance to property value, loan amount, and income,
 337 and lower importance on LTV ratio and DTI ratio.

338 The capability of g^{XNN} to model nonlinear phenomenon and high-degree interactions, and to do
 339 so in an interpretable manner, is on display in Figure 6. 6a presents the sparse γ_k weights of the g^{XNN}
 340 output layer in which the n_k subnetworks with $k \in \{0, 1, 2, 3, 5, 8, 9\}$ have large magnitude weights and
 341 n_k subnetworks, $k \in \{4, 6, 7\}$, have small or near-zero magnitude weights. Distinctive ridge functions
 342 that feed into those large magnitude γ_k weights are highlighted in 6b and color-coded to pair with
 343 their corresponding γ_k weight. As in the Subsection 2.1.2, n_k ridge function plots vary with the output
 344 of the corresponding projection layer $\sum_j \beta_{k,j} x_j$ hidden unit, with weights displayed in matching colors
 345 in 6c. In both the simulated and mortgage data, n_k ridge functions appear to be elementary functional
 346 forms that the output layer learns to combine to generate accurate predictions, reminiscent of basis
 347 functions for the modeled space. 6c displays the sparse β_j weights of the projection layer $\sum_j \beta_{k,j} x_j$
 348 hidden units that are associated with each n_k subnetwork ridge function. For instance, subnetwork
 349 n_3 is influenced by large weights for LTV ratio, no introductory rate period flag, and introductory
 350 rate period, whereas subnetwork n_9 is nearly completely dominated by the weight for income. See
 351 Appendix B.3 for details regarding general XNN architecture.

352 To compliment the global interpretability of g^{XNN} , Figure 7 displays local Shapley values for
 353 selected individuals, estimated from the projection layer using Deep SHAP in the g^{XNN} probability
 354 space. Similar to Tree SHAP, local Deep SHAP values should sum to $g^{\text{XNN}}(x)$. While the Shapley
 355 values appear to follow the roughly increasing pattern established in Figures A4, A6, and 4, their true
 356 value is their ability to be calculated for any $g^{\text{XNN}}(x)$ prediction, as a means to summarize model
 357 reasoning and allow for appeal and override of specific ML-based decisions, even for neural network
 358 architectures.

359 2.2.3. Discrimination Testing Results

360 Tables 3a and 3b show the results of the discrimination tests using the mortgage data for two sets
 361 of class-control groups: blacks as compared to whites, and females as compared to males. As with
 362 the simulated data in Table A1, several measures of disparities are shown, with the SMDs calculated
 363 using the probabilities from g^{MGBM} and g^{XNN} , and the accuracy, FPRs, and FPR ratios, MEs, and AIRs
 364 calculated using a binary outcome based on a cutoff of 0.20 (anyone with probabilities of 0.2 or less

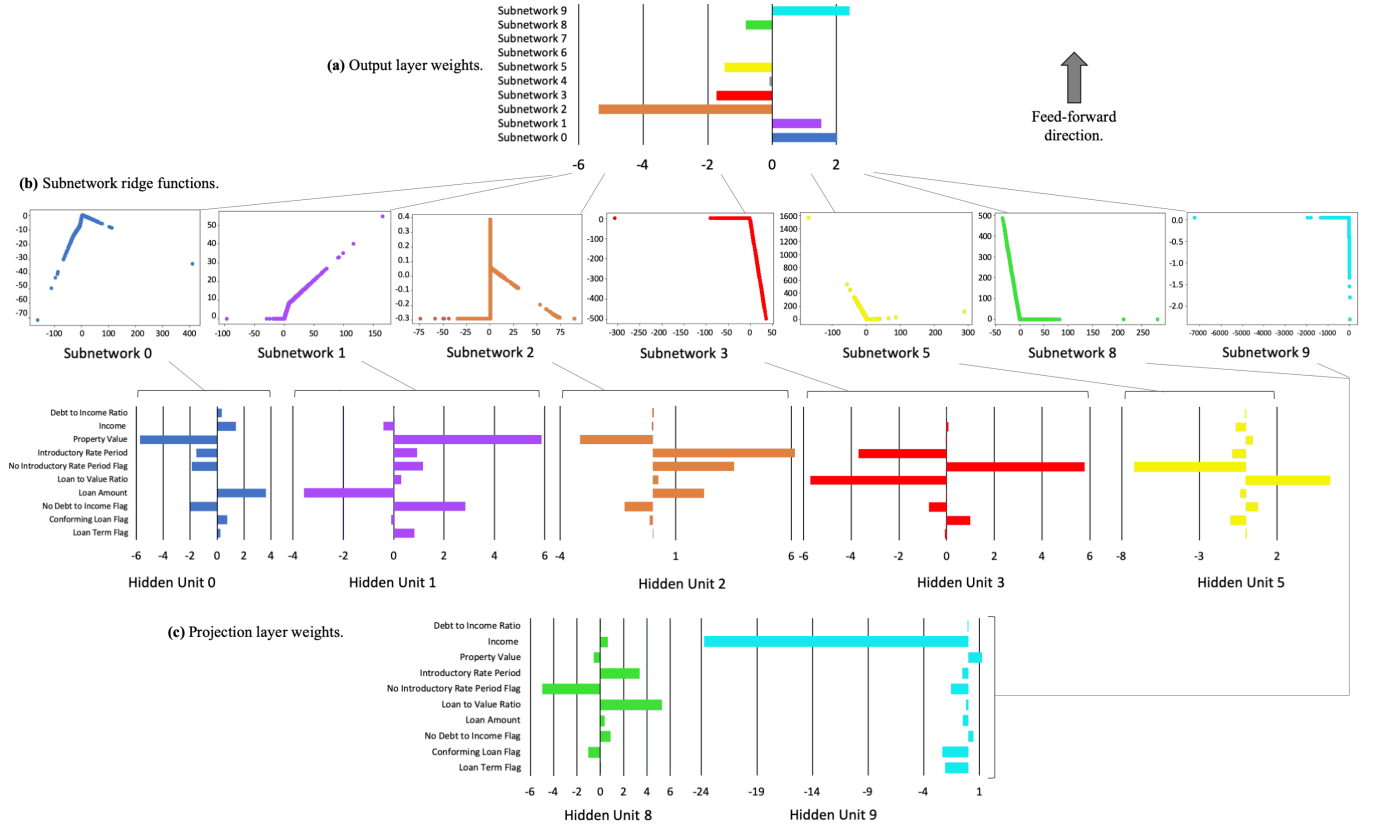


Figure 6. Output layer γ_k weights, corresponding n_k ridge functions, and associated projection layer β_j weights for g^{XNN} on the mortgage test data.

receives the favorable outcome).¹¹ Since g^{MGBM} and g^{XNN} are predicting the likelihood of receiving a high-priced loan, g^{MGBM} and g^{XNN} assume that a lower score is favorable. Thus, one might consider FPR ratios as a measure of the class-control disparities. FPR ratios are higher under g^{XNN} than g^{MGBM} (2.45 vs. 2.10) in Table 3b, but overall FPRs are lower for blacks under g^{XNN} (0.295 vs. 0.315) in Table 3a. This is the same pattern seen in the simulated data results in Appendix E.2, again leading to the question of whether a fairness goal should not only consider class-control relative rates, but also intra-class improvements in the chosen fairness metric. Similar results are found for the female-male comparison, but the relative rates are less stark: 1.15 for g^{MGBM} and 1.21 for g^{XNN} .

Both ME and AIR show higher disparities for blacks under g^{XNN} than g^{MGBM} . Blacks receive high-priced loans 21.4% more frequently using g^{XNN} vs. 18.3% for g^{MGBM} . Both g^{MGBM} and g^{XNN} show AIRs that are statistically significantly below parity (not shown, but available in resources discussed in Subsection 1.8), and which are also below the EEOC's 0.80 threshold. This would typically indicate need for further review to determine the cause and validity of these disparities, and a few relevant remediation techniques for such discovered discrimination are discussed in Subsection 3.3. On the other hand, women improve under g^{XNN} vs. g^{MGBM} (MEs of 3.6% vs. 4.1%; AIRs of 0.955 vs. 0.948). The AIRs, while statistically significantly below parity, are well above the EEOC's threshold of 0.80. In most situations, the values of these metrics alone would not likely flag a model for further review. Black SMDs for g^{XNN} and g^{MGBM} are similar: 0.621 and 0.628, respectively. These exceed Cohen's guidelines of 0.5 for a medium effect size and would likely trigger further review. Female

¹¹ See Appendix F for comments pertaining to discrimination testing and cutoff selection.

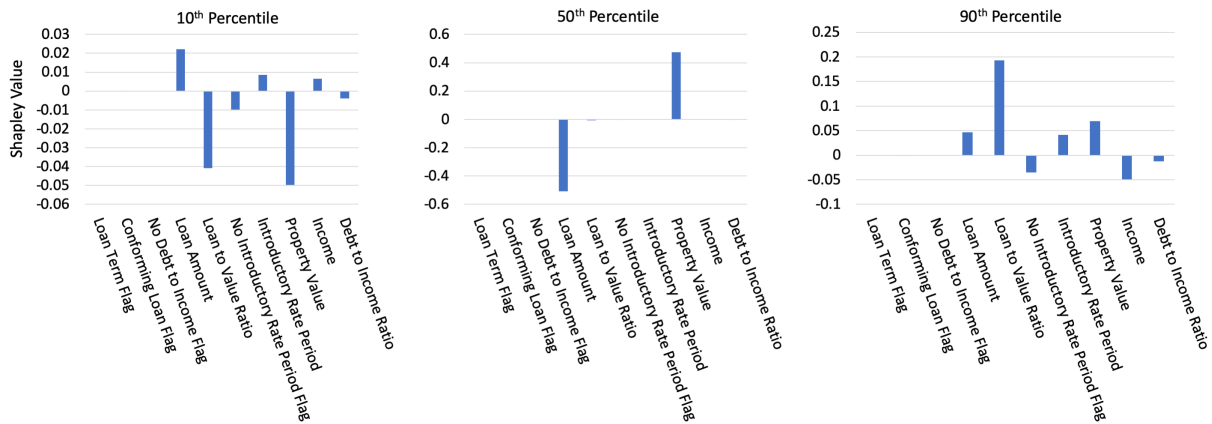


Figure 7. Deep SHAP values for three individuals across selected percentiles of $g^{XNN}(X)$ on the mortgage test data.

(a) Group size, accuracy, and FPR for g^{MGBM} and g^{XNN} on the mortgage test data.

Class	N	Model	Accuracy↑	FPR↓
Black	2,608	g^{MGBM}	0.654	0.315
		g^{XNN}	0.702	0.295
White	28,361	g^{MGBM}	0.817	0.150
		g^{XNN}	0.857	0.120
Female	8,301	g^{MGBM}	0.768	0.208
		g^{XNN}	0.822	0.158
Male	13,166	g^{MGBM}	0.785	0.182
		g^{XNN}	0.847	0.131

(b) AIR, ME, SMD, and FPR ratio for g^{MGBM} and g^{XNN} on the mortgage test data.

Model	Protected Class	Control Class	AIR↑	ME↓	SMD↓	FPR Ratio↓
g^{MGBM}	Black	White	0.776	18.3%	0.628	2.10
	Female	Male	0.948	4.1%	0.084	1.15
g^{XNN}	Black	White	0.743	21.4%	0.621	2.45
	Female	Male	0.955	3.6%	0.105	1.21

Table 3. Discrimination measures for the mortgage test data. Arrows indicate the direction of improvement for each measure.

384 SMDs are well below Cohen's definition of small effect size: 0.105 and 0.084 for g^{XNN} and g^{MGBM} ,
 385 respectively. Similar to results for female AIR, these values alone are unlikely to prompt further review.

3. Discussion

387 3.1. The Burgeoning Python Ecosystem for Responsible Machine Learning

388 Figure 8 displays a holistic approach to ML model training, assessment, deployment meant to
 389 decrease discrimination, inaccuracy, privacy, and security risks for high-stakes, human-centered, or
 390 regulated ML applications.¹² While all the methods mentioned in Figure 8 play an important role in
 391 increasing human trust and understanding of ML, a few pertinent references and Python resources are
 392 highlighted below as further reading to augment this this text's focus on certain interpretable models,
 393 post-hoc explanation, and discrimination testing techniques.

¹² See: [Toward Responsible Machine Learning](#) for details regarding Figure 8.

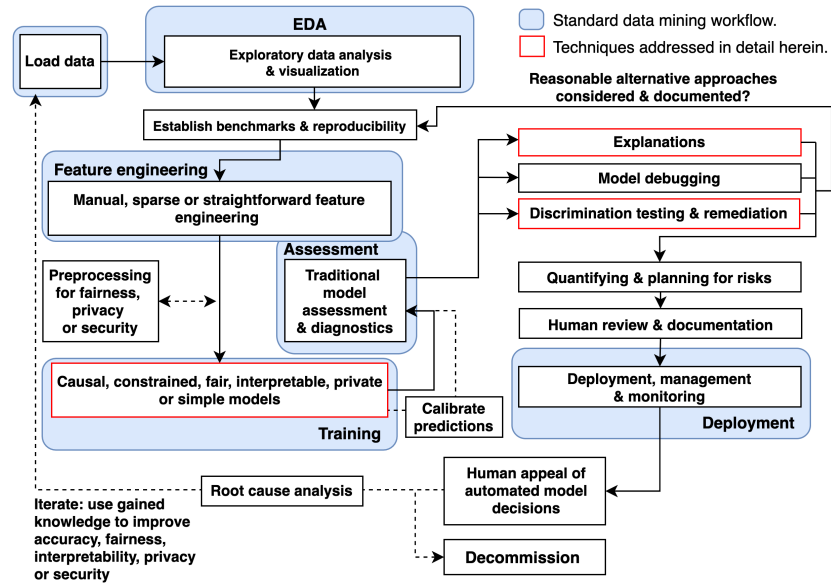


Figure 8. An example responsible ML workflow in which interpretable models, post-hoc explanations, discrimination testing and remediation techniques, among other review and appeal mechanisms, can create an understandable and trustworthy ML system.

Any discussion of interpretable ML models would be incomplete without references to the seminal work of the Rudin group at Duke University and EBM, or GA²M models, pioneered by researchers at Microsoft and Cornell. In keeping with a major theme of this manuscript, models from these leading researchers and several other kinds of interpretable ML models are now available as open source Python packages. Among several types of currently available interpretable models, practitioners can now use Python to evaluate EBM in the [interpret](#) package, optimal sparse decision trees, GAMs in the [pyGAM](#) package, a variant of Friedman's RuleFit in the [skope-rules](#) package, monotonic calibrated interpolated lookup tables in [tensorflow/lattice](#), and *this looks like that* interpretable deep learning [33], [34], [35], [36].^{13,14} Additional, relevant references and Python functionality include:

- **Exploratory data analysis (EDA):** H2OAggregatorEstimator in [h2o](#) [37].
- **Sparse feature extraction:** H2OGeneralizedLowRankEstimator in [h2o](#) [38].
- **Privacy preprocessing and private models:** differential privacy and private models in [diffprivlib](#) and [tensorflow/privacy](#) [39], [40], [41], [42].
- **Post-hoc explanation:** structured data explanations with [alibi](#) and [PDPbox](#), image classification explanations with [DeepExplain](#), and natural language explanations with [allenlp](#) [43], [44], [45].
- **Discrimination testing:** with [aequitas](#) and [Themis](#).
- **Discrimination remediation:** Reweighting, adversarial de-biasing, learning fair representations, and reject option classification with [AIF360](#) [46], [47], [48], [49].
- **Model debugging:** with [foolbox](#), [SALib](#), [tensorflow/cleverhans](#), and [tensorflow/model-analysis](#) [50], [51], [52], [53].
- **Model documentation:** models cards [54], e.g., [GPT-2 model card](#), [Object Detection model card](#).

See [Awesome Machine Learning Interpretability](#) for a longer, community-curated metalist of related software packages and resources.

¹³ See: [Optimal sparse decision trees](#).

¹⁴ See: [This looks like that](#) interpretable deep learning.

417 3.2. *Appeal and Override of Automated Decisions*

418 Interpretable models and post-hoc explanations play an important role in increasing transparency
419 into model mechanisms and predictions. As seen in Section 2, interpretable models often enable
420 users to enforce domain knowledge-based constraints on model behavior, to ensure that models obey
421 reasonable expectations, and to gain data-derived insights into the modeled problem domain. Post-hoc
422 explanations generally help describe and summarize mechanisms and decisions, potentially yielding
423 an even clearer understanding of ML models. Together they can allow for human learning from ML,
424 certain types of regulatory compliance, and crucially, human appeal or override of automated model
425 decisions [31]. Interpretable models and post-hoc explanations are likely good candidates for ML uses
426 cases under the FCRA, ECOA, GDPR and other regulations that may require explanations of model
427 decisions, and they are already used in the financial services industry today for model validation and
428 other purposes.^{15,16} Writ large, transparency in ML also facilitates additional responsible AI processes
429 such as model debugging, model documentation, and logical appeal and override processes, some of
430 which may also be required by applicable regulations.¹⁷ Among these, providing persons affected by a
431 model with the opportunity to appeal ML-based decisions may deserve the most attention. ML models
432 are often wrong¹⁸ and appealing black-box decisions can be difficult.² For high-stakes, human-centered,
433 or regulated applications that are trusted with mission- or life-critical decisions, the ability to logically
434 appeal or override inevitable wrong decisions is not only a possible prerequisite for compliance, but
435 also a failsafe procedure for those affected by ML decisions.

436 3.3. *Discrimination Testing and Remediation in Practice*

437 A significant body of research has emerged around exploring and fixing algorithmic
438 discrimination [56]. Broadly, methodologies can be placed into two groups: more traditional methods
439 that mitigate discrimination by searching across possible algorithmic and feature specifications, and
440 more recently developed approaches that change the algorithms or input data themselves in order
441 to mitigate disparities. Many approaches that have been developed in the last 5–7 years focus on
442 altering the algorithm itself, preprocessing training data, or post-processing predictions in order to
443 diminish class-control correlations or dependencies. Whether these more recent methods are suitable
444 for a particular use case depends on the legal environment in which the model is deployed and on the
445 use case itself. For comments on why these techniques could result in regulatory non-compliance in
446 certain scenarios, see Appendix G.

447 Of the newer class of fairness enhancing interventions, within-algorithm discrimination mitigation
448 techniques that do not use class information may be more likely to be acceptable in highly regulated
449 settings today. These techniques often work by incorporating a loss function where more discriminatory
450 paths or weights are penalized and will only be used by the model if improvements in model fit
451 overcome the penalty. (The relative level of fit-to-discrimination penalty is usually determined via
452 a hyperparameter choice.) Other mitigation strategies that only alter hyperparameters or algorithm
453 choice are also likely to be acceptable. And feature selection techniques that have been used in
454 traditional modeling (e.g., linear models and decision trees) are likely to continue to be accepted in
455 regulatory environments. For further discussion of potential and utilized techniques that can mitigate
456 DI in US financial services, see Schmidt and Stephens [57].

15 See: *Deep Insights into Explainability and Interpretability of Machine Learning Algorithms and Applications to Risk Management*.

16 Unfortunately, many non-consistent explanation methods can result in drastically different global and local feature importance values across different models trained on the same data or even for refreshing a model with augmented training data [32]. Consistency and accuracy guarantees are perhaps a factor in the growing momentum behind Shapley values as a candidate technique for generating consumer-specific adverse action notices for explaining and appealing automated ML-based decisions in highly-regulated settings, such as credit lending [55].

17 E.g.: [US Federal Reserve Bank Supervision and Regulation \(SR\) Letter 11-7: Guidance on Model Risk Management](#).

18 "All models are wrong, but some are useful." – George Box, Statistician (1919 - 2013)

457 Regardless of the methodology chosen to minimize disparities, advances in computing have
458 enhanced the ability to search for less discriminatory models. Prior to these advances, only a small
459 number of alternative algorithms could be tested for lower levels of disparity without causing infeasible
460 delays in model implementation. Now, large numbers of models can be quickly tested for lower
461 discrimination and better predictive quality. An additional opportunity arises as a result of ML itself:
462 the well-known Rashomon effect, or the multiplicity of good ML models for most datasets. It is now
463 feasible to train more models, find more good models, and test more models for discrimination, and
464 among all those tested models, there are likely to be some with high predictive performance and low
465 discrimination.

466 3.4. Intersectional and Non-static Risks in Machine Learning

467 The often black-box nature of ML, the perpetuation or exacerbation of discrimination by ML, or
468 the privacy harms and security vulnerabilities inherent in ML are each serious and difficult problems on
469 their own. However, evidence is mounting that these harms can also manifest as complex intersectional
470 challenges, e.g., the *fairwashing* or *scaffolding* of biased models with ML explanations, the privacy harms
471 of ML explanations, or the adversarial poisoning of ML models to become discriminatory [8], [18],
472 [19].^{19,20,21} Practitioners should of course consider the discussed interpretable modeling, post-hoc
473 explanation, and discrimination testing approaches as at least partial remedies to the black-box and
474 discrimination issues in ML. However, they should also consider that explanations can ease model
475 stealing, data extraction, and membership inference attacks, and that explanations can mask ML
476 discrimination. Additionally, high-stakes, human-centered, or regulated ML systems should generally
477 be built and tested with robustness to adversarial attacks as a primary design consideration, and
478 specifically to prevent ML models from being poisoned or otherwise altered to become discriminatory.
479 Accuracy, discrimination, and security characteristics of a system can change over time as well. Simply
480 testing for these problems at training time, as presented in Section 2, is not adequate for high-stakes,
481 human-centered, or regulated ML systems. Accuracy, discrimination, and security should be monitored
482 in real-time and over time, as long as a model is deployed.

483 4. Conclusion

484 This text puts forward results on simulated data to provide some validation of constrained ML
485 models, post-hoc explanation techniques, and discrimination testing methods. These same modeling,
486 explanation, and discrimination testing approaches are then applied to more realistic mortgage data
487 to provide an example of a responsible ML workflow for high-stakes, human-centered, or regulated
488 ML applications. The discussed methodologies are solid steps toward interpretability, explanation,
489 and minimal discrimination for ML decisions, which should ultimately enable increased fairness
490 and logical appeal processes for ML decision subjects. Of course, there is more to the responsible
491 practice of ML than interpretable models, post-hoc explanation, and discrimination testing, even from
492 a technology perspective, and Section 3 also points out numerous additional references and open
493 source Python software assets that are available to researchers and practitioners today to increase
494 human trust and understanding in ML systems. While the complex and messy problems of racism,
495 sexism, privacy violations, and cyber crime can probably never be solved by technology alone, this
496 work (and many others) illustrate numerous ways for ML practitioners to mitigate such risks.

¹⁹ See: [Tay, Microsoft's AI chatbot, gets a crash course in racism from Twitter](#).

²⁰ While the focus of this paper is not ML security, proposed best-practices from that field do point to transparency of ML systems as a mitigating factor for some ML attacks and hacks [53]. High system complexity is sometimes considered a mitigating influence as well [58]. This is sometimes known as the *transparency paradox* in data privacy and security, and it likely applies to ML security as well, especially in the context of interpretable ML models and post-hoc explanation.

²¹ See: [The AI Transparency Paradox](#).

497 Author Contributions: NG, data cleaning, GBM and MGBM assessment and results; PH, primary author; KM,
498 ANN and XNN implementation, assessment, and results; NS, secondary author, data simulation and collection,
499 and discrimination testing.

500 Funding: This work received no external funding.

501 Acknowledgments: Wen Phan for work in formalizing notation. Sue Shay for editing. Andrew Burt for ideas
502 around the transparency paradox.

503 Conflicts of Interest: XNN was first made public by the corporate model validation team at Wells Fargo bank.
504 Wells Fargo is a customer of, and investor in, H2O.ai and a client of BLDS, LLC. However, communications
505 regarding XNN between Wells Fargo and the authors have been extremely limited prior to and during the drafting
506 of this manuscript. Moreover, Wells Fargo exerted absolutely no editorial control over the text or results herein.

507 Abbreviations

508 The following abbreviations are used in this text: AI – artificial intelligence, AIR - adverse impact ratio, ALE -
509 accumulated local effect, ANN – artificial neural network, APR – annual percentage rate, AUC – area under the
510 curve, CFPB – Consumer Financial Protection Bureau, DI – disparate impact, DT – disparate treatment, DTI – debt
511 to income, EBM or GA²M – explainable boosting machine, i.e. variants GAMs that consider two-way interactions
512 and may incorporate boosting into training, EEOC – Equal Employment Opportunity Commission, ECOA -
513 Equal Credit Opportunity Act, EDA – exploratory data analysis, EU – European Union, FCRA – Fair Credit
514 Reporting Act, FNR – false negative rate, FPR – false positive rate, GAM – generalized additive model, GBM –
515 gradient boosting machine, GDPR - General Data Protection Regulation, HMDA – Home Mortgage Disclosure
516 Act, ICE – individual conditional expectation, LTV – loan to value, MCC – Matthews correlation coefficient, ME –
517 marginal effect, MGBM – monotonic gradient boosting machine, ML – machine learning, PD – partial dependence,
518 RMSE – root mean square error, SGD – stochastic gradient descent, SHAP – SHapley Additive exPlanation, SMD -
519 standardized mean difference, SR – supervision and regulation, US – United States, XNN – explainable neural
520 network.

521 Appendix A. Mortgage Data Details

522 The US HMDA law, originally enacted in 1975, requires many financial institutions that originate
523 mortgage products to provide certain data about many of the mortgage-related products that they
524 either deny or originate on an annual basis. This information is first provided to the CFPB, which
525 subsequently releases some of the data to the public. Regulators often use HMDA data to, "...show
526 whether lenders are serving the housing needs of their communities; they give public officials
527 information that helps them make decisions and policies; and they shed light on lending patterns that
528 could be discriminatory."⁵ In addition to regulatory use, public advocacy groups use these data for
529 similar purposes, and the lenders themselves use the data to benchmark their community outreach
530 relative to their peers. The publicly available data that the CFPB releases includes information such as
531 the lender, the type of loan, loan amount, LTV ratio, DTI ratio, and other important financial descriptors.
532 The data also include information on each borrower and co-borrower's race, ethnicity, gender, and
533 age. Because the data includes information on these protected class characteristics, certain metrics
534 that can be indicative of discrimination in lending can be calculated directly using the HDMA data.
535 Ultimately, the HMDA data represent the most comprehensive source of data on highly-regulated
536 mortgage lending that is publicly available, which makes it an ideal dataset to use for the types of
537 analyses set forth in Sections 1 and 2.

538 Appendix B. Selected Algorithmic Details

539 Appendix B.1. Notation

540 To facilitate descriptions of data and modeling, explanatory, and discrimination testing techniques,
541 notation for input and output spaces, datasets, and models is defined.

542 Appendix B.1.1. Spaces

- 543 • Input features come from the set \mathcal{X} contained in a P -dimensional input space, $\mathcal{X} \subset \mathbb{R}^P$. An
 544 arbitrary, potentially unobserved, or future instance of \mathcal{X} is denoted $\mathbf{x}, \mathbf{x} \in \mathcal{X}$.
 545 • Labels corresponding to instances of \mathcal{X} come from the set \mathcal{Y} .
 546 • Learned output responses of models are contained in the set $\hat{\mathcal{Y}}$.

547 Appendix B.1.2. Data

- 548 • The input dataset \mathbf{X} is composed of observed instances of the set \mathcal{X} with a corresponding dataset
 549 of labels \mathbf{Y} , observed instances of the set \mathcal{Y} .
 550 • Each i -th observation of \mathbf{X} is denoted as $\mathbf{x}^{(i)} = [x_0^{(i)}, x_1^{(i)}, \dots, x_{P-1}^{(i)}]$, with corresponding i -th labels
 551 in \mathbf{Y} , $\mathbf{y}^{(i)}$, and corresponding predictions in $\hat{\mathbf{Y}}, \hat{\mathbf{y}}^{(i)}$.
 552 • \mathbf{X} and \mathbf{Y} consist of N tuples of observations: $[(\mathbf{x}^{(0)}, \mathbf{y}^{(0)}), (\mathbf{x}^{(1)}, \mathbf{y}^{(1)}), \dots, (\mathbf{x}^{(N-1)}, \mathbf{y}^{(N-1)})]$.
 553 • Each j -th input column vector of \mathbf{X} is denoted as $X_j = [x_j^{(0)}, x_j^{(1)}, \dots, x_j^{(N-1)}]^T$.

554 Appendix B.1.3. Models

- 555 • A type of ML model g , selected from a hypothesis set \mathcal{H} , is trained to represent an unknown
 556 signal-generating function f observed as \mathbf{X} with labels \mathbf{Y} using a training algorithm $\mathcal{A}: \mathbf{X}, \mathbf{Y} \xrightarrow{\mathcal{A}} g$,
 557 such that $g \approx f$.
 558 • g generates learned output responses on the input dataset $g(\mathbf{X}) = \hat{\mathbf{Y}}$, and on the general input
 559 space $g(\mathcal{X}) = \hat{\mathcal{Y}}$.
 560 • The model to be explained and tested for discrimination is denoted as g .

561 Appendix B.2. Monotonic Gradient Boosting Machine Details

562 As in unconstrained GBM, Θ_b^{mono} is selected in a greedy, additive fashion by minimizing a regularized
 563 loss function that considers known target labels, \mathbf{y} , the predictions of all subsequently trained trees
 564 in the in $g^{\text{MGBM}}, g_{b-1}^{\text{MGBM}}(\mathbf{X})$, and the b -th tree splits, $T_b(\mathbf{x}^{(i)}; \Theta_b^{\text{mono}})$, in a numeric error function (e.g.,
 565 squared error, Huber error), l , and a regularization term that penalizes complexity in the current tree,
 566 $\Omega(T_b)$. For the b -th iteration, the loss function, \mathcal{L}_b , can generally be defined as:

$$\mathcal{L}_b = \sum_{i=0}^{N-1} l(y^{(i)}, g_{b-1}^{\text{MGBM}}(\mathbf{x}^{(i)}), T_b(\mathbf{x}^{(i)}; \Theta_b^{\text{mono}})) + \Omega(T_b) \quad (\text{A1})$$

567 In addition to \mathcal{L}_b , g^{MGBM} training is characterized by additional splitting rules and constraints on
 568 tree node weights. Each binary splitting rule, $\theta_{b,j,k} \in \Theta_b$, is associated with a feature, X_j , is the
 569 k -th split associated with X_j in T_b , and results in left and right child nodes with a numeric weights,
 570 $\{w_{b,j,k,L}, w_{b,j,k,R}\}$. For terminal nodes, $\{w_{b,j,k,L}, w_{b,j,k,R}\}$ can be direct numeric components of some
 571 g^{MGBM} prediction. For two values of some feature X_j , $x_j^\alpha \leq x_j^\beta$, g^{MGBM} is positive monotonic with
 572 respect to some X_j if $g^{\text{MGBM}}(x_j^\alpha) \leq g^{\text{MGBM}}(x_j^\beta) \forall x_j^\alpha \leq x_j^\beta \in X_j$. The following rules and constraints
 573 ensure positive monotonicity in Θ_b , where the prediction for each value results in $T_b(x_j^\alpha; \Theta_b) = w_\alpha$
 574 and $T_b(x_j^\beta; \Theta_b) = w_\beta$.

- 575 1. For the first and highest split in T_b involving X_j , any $\theta_{b,j,0}$ resulting in $T(x_j; \theta_{b,j,0}) = \{w_{b,j,0,L}, w_{b,j,0,R}\}$ where $w_{b,j,0,L} > w_{b,j,0,R}$, is not considered.
- 576 2. For any subsequent left child node involving X_j , any $\theta_{b,j,k \geq 1}$ resulting in $T(x_j; \theta_{b,j,k \geq 1}) = \{w_{b,j,k \geq 1,L}, w_{b,j,k \geq 1,R}\}$ where $w_{b,j,k \geq 1,L} > w_{b,j,k \geq 1,R}$, is not considered.
- 577 3. Moreover, for any subsequent left child node involving X_j , $T(x_j; \theta_{b,j,k \geq 1}) = \{w_{b,j,k \geq 1,L}, w_{b,j,k \geq 1,R}\}$,
 578 $\{w_{b,j,k \geq 1,L}, w_{b,j,k \geq 1,R}\}$ are bound by the associated $\theta_{b,j,k-1}$ set of node weights,
 579 $\{w_{b,j,k-1,L}, w_{b,j,k-1,R}\}$, such that $\{w_{b,j,k \geq 1,L}, w_{b,j,k \geq 1,R}\} < \frac{w_{b,j,k-1,L} + w_{b,j,k-1,R}}{2}$.
- 580 4. (1) and (2) are also applied to all right child nodes, except that for right child nodes $w_{b,j,k,L} \leq w_{b,j,k,R}$ and
 581 $\{w_{b,j,k \geq 1,L}, w_{b,j,k \geq 1,R}\} \geq \frac{w_{b,j,k-1,L} + w_{b,j,k-1,R}}{2}$.

584 Note that for any one X_j and $T_b \in g^{\text{MGBM}}$ left subtrees will always produce lower predictions than
 585 right subtrees, and that any $g^{\text{MGBM}}(\mathbf{x})$ is an addition of each T_b output, with the application of
 586 a monotonic logit or softmax link function for classification problems. Moreover, each tree's root
 587 node corresponds to some constant node weight that by definition obeys monotonicity constraints,
 588 $T(x_j^\alpha; \theta_{b,0}) = T(x_j^\beta; \theta_{b,0}) = w_{b,0}$. Together these additional splitting rules and node weight constraints
 589 ensure that $g^{\text{MGBM}}(x_j^\alpha) \leq g^{\text{MGBM}}(x_j^\beta) \forall x_j^\alpha \leq x_j^\beta \in X_j$. For a negative monotonic constraint, i.e.,
 590 $g^{\text{MGBM}}(x_j^\alpha) \geq g^{\text{MGBM}}(x_j^\beta) \forall x_j^\alpha \leq x_j^\beta \in X_j$, left and right splitting rules and node weight constraints are
 591 switched. Also consider that MGBM models with independent monotonicity constraints between some
 592 X_j and \mathbf{y} likely restrict non-monotonic interactions between multiple X_j . Moreover, if monotonicity
 593 constraints are not applied to all $X_j \in \mathbf{X}$, any strong non-monotonic signal in training data associated
 594 with some important X_j may be forced onto some other arbitrary unconstrained X_j under some g^{MGBM}
 595 models, compromising the end goal of interpretability.

596 *Appendix B.3. Explainable Neural Network Details*

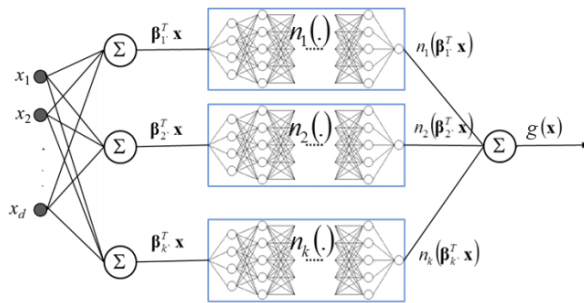


Figure A1. A diagram of an XNN with three meta-layers: the bottom combination layer with K linear $\sum_j \beta_{k,j} x_j$ hidden units, the middle meta-layer with K hidden and separate n_k ridge functions, and the output combination layer that generates g^{XNN} predictions. Figure adapted from Vaughan *et al.* [20].

597 g^{XNN} is comprised of 3 meta-layers:

- 598 1. The first and deepest meta-layer, composed of K linear $\sum_j \beta_{k,j} x_j$ hidden units, which should learn
 599 higher magnitude weights for important X_j , is known as the *projection layer*. It is fully connected
 600 to each input X_j . Each hidden unit in the projection layer may optionally include a bias term.
- 601 2. The second meta-layer contains K hidden and separate n_k ridge functions, or *subnetworks*. Each
 602 n_k is a neural network, which can be parameterized to suit a given modeling task. To facilitate
 603 direct interpretation and visualization, the input to each subnetwork is the 1-dimensional output
 604 of its associated projection layer hidden unit, $\sum_j \beta_{k,j} x_j$. Each n_k can contain several bias terms.
- 605 3. The output meta-layer, called the *combination layer*, is another linear unit comprised of a global bias
 606 term, μ_0 , and the K weighted 1-dimensional outputs of each subnetwork, $\gamma_k n_k(\sum_j \beta_{k,j} x_j)$. Again,
 607 subnetwork output is restricted to 1-dimension for interpretation and visualization purposes.

608 *Appendix B.4. One-dimensional Partial Dependence and Individual Conditional Expectation Details*

609 Following Friedman *et al.* [13] a single feature $X_j \in \mathbf{X}$ and its complement set $\mathbf{X}_{\mathcal{P} \setminus \{j\}} \in \mathbf{X}$ (where
 610 $X_j \cup \mathbf{X}_{\mathcal{P} \setminus \{j\}} = \mathbf{X}$) is considered. $\text{PD}(X_j, g)$ for a given feature X_j is estimated as the average output of
 611 the learned function $g(\mathbf{X})$ when all the observations of X_j are set to a constant $x \in \mathcal{X}$ and $\mathbf{X}_{\mathcal{P} \setminus \{j\}}$ is left
 612 unchanged. $\text{ICE}(x_j, g)$ for a given instance \mathbf{x} and feature x_j is estimated as the output of $g(\mathbf{x})$ when x_j
 613 is set to a constant $x \in \mathcal{X}$ and all other features $\mathbf{x} \in \mathbf{X}_{\mathcal{P} \setminus \{j\}}$ are left untouched. PD and ICE curves are
 614 usually plotted over some set of constants $x \in \mathcal{X}$, as displayed in Subsection 2.2.2 and Appendix E.1.
 615 Due to known problems for PD in the presence of strong correlation and interactions, PD should not
 616 be used alone. PD should be paired with ICE or be replaced with accumulated local effect (ALE) plots
 617 [22], [29].

618 **Appendix B.5. Shapley Value Details**

619 For some instance $\mathbf{x} \in \mathcal{X}$, Shapley explanations take the form:

$$g(\mathbf{x}) = \phi_0 + \sum_{j=0}^{j=\mathcal{P}-1} \phi_j \mathbf{z}_j \quad (\text{A2})$$

620 In Equation A2, $\mathbf{z} \in \{0,1\}^{\mathcal{P}}$ is a binary representation of \mathbf{x} where 0 indicates missingness. Each ϕ_j
 621 is the local feature contribution value associated with x_j , and ϕ_0 is the average of $g(\mathbf{X})$. Each ϕ_j is a
 622 weighted combination of model scores, $g_x(\mathbf{x})$, with x_j , $g_x(S \cup \{j\})$, and the model scores without x_j ,
 623 $g_x(S)$, for every subset of features S not including j , $S \subseteq \mathcal{P} \setminus \{j\}$, where g_x incorporates the mapping
 624 between \mathbf{x} and the binary vector \mathbf{z} .

$$\phi_j = \sum_{S \subseteq \mathcal{P} \setminus \{j\}} \frac{|S|!(\mathcal{P} - |S| - 1)!}{\mathcal{P}!} [g_x(S \cup \{j\}) - g_x(S)] \quad (\text{A3})$$

625 Local, per-instance explanations using Shapley values tend to involve ranking x_j by ϕ_j values or
 626 delineating a set of the X_j names associated with the k -largest ϕ_j values for some \mathbf{x} , where k is some
 627 small positive integer, say 5. Global explanations are typically the absolute mean of the ϕ_j associated
 628 with a given X_j across all of the observations in some set \mathbf{X} .

629 **Appendix C. Types of Machine Learning Discrimination in US Legal and Regulatory Settings**

630 It is important to explain and draw a distinction between the two major types of discrimination
 631 recognized in US legal and regulatory settings, disparate treatment (DT), and disparate impact (DI).
 632 DT (which is loosely referred to as *intentional discrimination*) occurs most often in an algorithmic setting
 633 when a model explicitly uses protected class status (e.g., race, sex) as an input feature or uses a feature
 634 that is so similar to protected class status that it essentially proxies for class membership. With some
 635 limited exceptions, the use of these factors in an algorithm is illegal under several statutes in the US.⁴
 636 DI, colloquially known as *unintentional discrimination*, occurs when some element of a decisioning
 637 process includes a *facially neutral* factor (i.e., a reasonable and valid predictor of response) that results
 638 in a disproportionate share of a protected class receiving an unfavorable outcome. In modeling, this is
 639 most typically driven by a statistically important feature that is distributed unevenly across classes,
 640 which causes more frequent unfavorable outcomes for the protected class. However, other factors,
 641 such as hyperparameter or algorithm choices, can drive DI. Crucially, legality hinges on whether
 642 changing the model, for example exchanging one feature for another or altering the hyperparameters
 643 of an algorithm, can lead to a similarly predictive model with lower DI.

644 **Appendix D. Practical vs. Statistical Significance for Discrimination Testing**

645 A finding of *practical significance* means that discovered disparity is not only statistically significant,
 646 but also passes beyond a chosen threshold that would constitute *prima facia* evidence of illegal
 647 discrimination. Practical significance acknowledges that any large dataset is likely to show statistically
 648 significant differences in outcomes by class, even if those differences are not truly meaningful. It further
 649 recognizes that there are likely to be situations where differences in outcomes are beyond a model
 650 user's ability to correct them without significantly degrading the quality of the model. Moreover,
 651 practical significance is also needed by model builders and compliance personnel to determine whether
 652 a model should undergo remediation efforts before it is put into production. Unfortunately, guidelines
 653 for practical significance, i.e., the threshold at which any statistically significant disparity would
 654 be considered evidence of illegal discrimination, are not as frequently codified as the standards for
 655 statistical significance. One exception, however, is in employment discrimination analyses, where the
 656 US Equal Employment Opportunity Commission (EEOC) has stated that if the AIR is below 0.80 and
 657 statistically significant, then this constitutes *prima facia* evidence of discrimination, which the model

658 user must rebut in order for the DI not to be considered illegal discrimination.²² It is important to
 659 note that the 0.80 measure of practical significance, also known as the *80% rule* and the *4/5ths rule*, is
 660 explicitly used in relation to AIR, and it is not clear that the use of this threshold is directly relevant to
 661 testing fairness for measures other than the AIR.

662 The legal thresholds for determining statistical significance is clearer and more consistent than that
 663 for practical significance. The first guidance in US courts occurred in a case involving discrimination
 664 in jury selection, *Castaneda vs. Partida*.²³ Here, the US Supreme Court wrote that, “As a general rule for
 665 such large samples, if the difference between the expected value and the observed number is greater
 666 than two or three standard deviations, then the hypothesis that the jury drawing was random would
 667 be suspect to a social scientist.” This “two or three standard deviations” test was then applied to
 668 employment discrimination in *Hazelwood School Districts vs. United States*.²⁴ Out of this, a 5% two-sided
 669 test ($z=1.96$), or an equivalent 2.5% one-sided test, has become a common standard for determining
 670 whether evidence of disparities is statistically significant.

671 Appendix E. Additional Simulated Data Results

672 As seen in Subsection 2.1.1, little or no trade-off is required in terms of model to fit to use the
 673 constrained models. Hence, intrinsic interpretability, post-hoc explainability, and discrimination are
 674 explored further for the g^{MGBM} and g^{XNN} models in Appendices E.1 - E.2. Intrinsic interpretability for
 675 g^{MGBM} is evaluated with PD and ICE, and post-hoc explainability is highlighted via global and local
 676 Shapley explanations. For g^{XNN} , Shapley explanation techniques are also used to generate global and
 677 local feature importance to augment interpretability results exhibited in Subection 2.1.2. Both g^{MGBM}
 678 and g^{XNN} are evaluated for discrimination using AIR, ME, SMD, and other measures.

679 Appendix E.1. Interpretability and Post-hoc Explanation Results

680 Global mean absolute Shapley value feature importance for $g^{\text{MGBM}}(\mathbf{X})$ on the simulated test data
 681 is displayed in Figure A2.

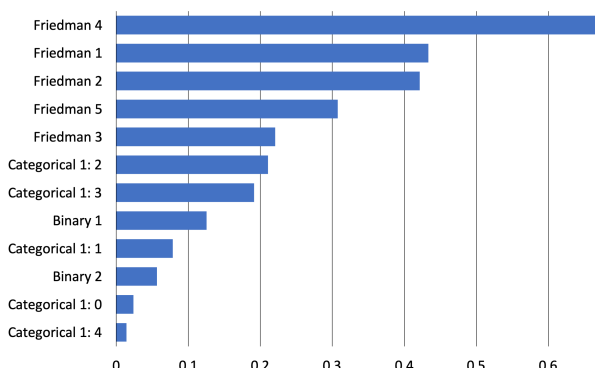


Figure A2. Global mean absolute Tree SHAP feature importance for $g^{\text{MGBM}}(\mathbf{X})$ on the simulated test data.

682 As expected, the $X_{\text{Friedman},j}$ features from the original Friedman [10] and Friedman *et al.* [11] formula
 683 are the main drivers of $g^{\text{MGBM}}(\mathbf{X})$ predictions, with encoded versions of the augmented categorical
 684 and binary features contributing less on average to $g^{\text{MGBM}}(\mathbf{X})$ predictions.

685 Figure A3 highlights PD, ICE, and histograms of the most important features from Figure A2.

22 Importantly, the standard of 0.80 is not a law, but a rule of thumb for agencies tasked with enforcement of discrimination laws. “Adoption of Questions and Answers To Clarify and Provide a Common Interpretation of the Uniform Guidelines on Employee Selection Procedures,” Federal Register, Volume 44, Number 43 (1979).

23 *Castaneda vs. Partida*, 430 US 482 - Supreme Court (1977)

24 *Hazelwood School Dist. vs. United States*, 433 US 299 (1977)

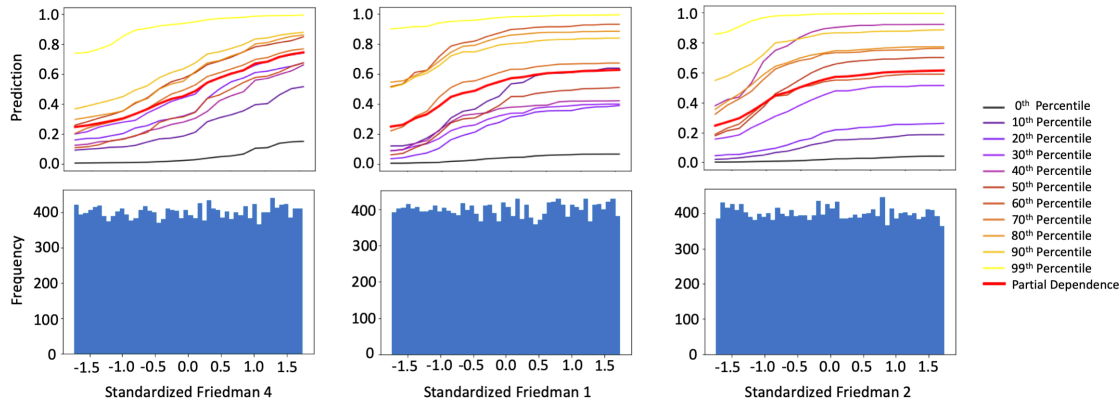


Figure A3. PD, ICE for 10 observations across selected percentiles of $g^{\text{MGBM}}(\mathbf{X})$, and histograms for the three most important input features of g^{MGBM} on the simulated test data.

686 $X_{\text{Friedman},1}$, $X_{\text{Friedman},2}$, and $X_{\text{Friedman},4}$ were positively monotonically constrained under g^{MGBM}
 687 for the simulated data, and positive monotonicity looks to be confirmed on average with PD and at
 688 numerous local percentiles of $g^{\text{MGBM}}(\mathbf{X})$ with ICE. Also, as the PD curves generally follow the patterns
 689 of the ICE curves, PD is likely an accurate representation of average feature behavior for $X_{\text{Friedman},1}$,
 690 $X_{\text{Friedman},2}$, and $X_{\text{Friedman},4}$. Since PD and ICE curves do not obviously diverge, g^{MGBM} is probably not
 691 modeling strong interactions, despite the fact that known interactions are included in the simulated
 692 data signal generating function in Equation 1. The one-dimensional monotonic constraints may hinder
 693 the modeling of such interactions, but do not strongly affect overall g^{MGBM} accuracy, perhaps due to
 694 noise in the simulated data. This is an interesting result for responsible ML practitioners. In some
 695 noisy scenarios, monotonicity constraints can increase model interpretability without causing a drastic
 696 drop in model accuracy, even when known interactions and non-monotonic behavior exist in training
 697 data.

698 Local Shapley values for records at the 10th, 50th, and 90th percentiles of $g^{\text{MGBM}}(\mathbf{X})$ in the
 699 simulated test data are displayed in Figure A4.

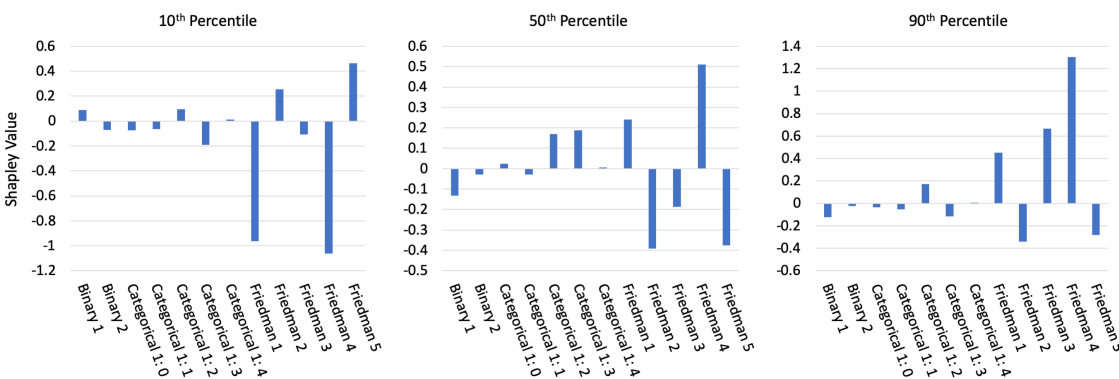


Figure A4. Tree SHAP values for three observations across selected percentiles of $g^{\text{MGBM}}(\mathbf{X})$ for the simulated test data.

700 The Shapley values in Figure A4 appear to be a logical result. For the lower prediction at the
 701 10th percentile of $g^{\text{MGBM}}(\mathbf{X})$, the largest local contributions are negative and the majority of local
 702 contributions are also negative. At the median of $g^{\text{MGBM}}(\mathbf{X})$, local contributions are roughly split
 703 between positive and negative values, and at the 90th of $g^{\text{MGBM}}(\mathbf{X})$, most large contributions are
 704 positive. In each case, large local contributions generally follow global importance results in Figure A2
 705 as well.

706 Figure A5 shows global mean absolute Shapley feature importance for g^{XNN} on the simulated
707 test data, using the approximate Deep SHAP technique.

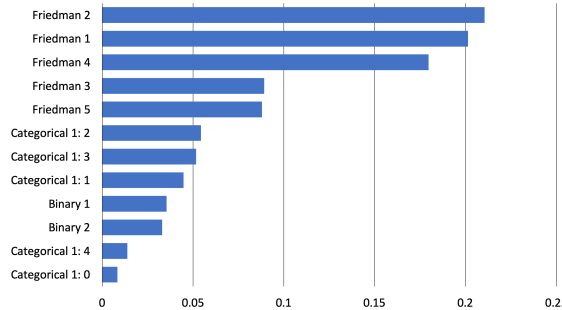


Figure A5. Global mean Deep SHAP feature importance for $g^{XNN}(X)$ on the simulated test data.

708 Like g^{MGBM} , g^{XNN} ranks the $X_{Friedman,j}$ features higher in terms of importance than the categorical
709 and binary features. The consistency between the feature rankings of g^{MGBM} and g^{XNN} is somewhat
710 striking, given their different hypothesis families and architectures. Both g^{MGBM} and g^{XNN} rank
711 $X_{Friedman,1}$, $X_{Friedman,2}$, and $X_{Friedman,4}$ as the most important features, both place $X_{Categorical,2}$ and
712 $X_{Categorical,3}$ above the $X_{Binary,1}$ and $X_{Binary,2}$ features, both rank $X_{Binary,1}$ above $X_{Binary,2}$, and both
713 place the least importance on $X_{Categorical,4}$ and $X_{Categorical,0}$.

714 Local Deep SHAP feature importance in Figure A6 supplements the global interpretability of
715 g^{XNN} displayed in Figures A5 and 1. Local Deep SHAP values are extracted from the projection layer
716 of g^{XNN} and reported in the probability space. Deep SHAP values can be calculated for any arbitrary
717 $g^{XNN}(x)$, allowing for detailed, local summarization of individual model predictions.

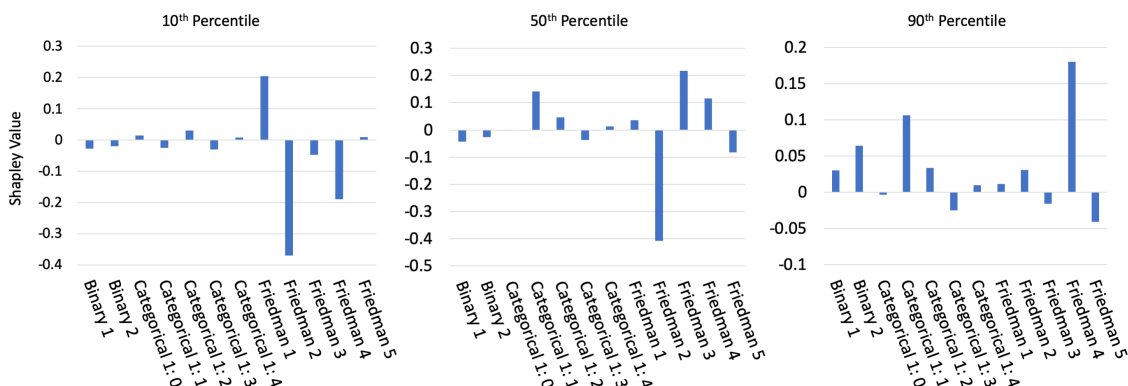


Figure A6. Deep SHAP values for three observations across selected percentiles of $g^{XNN}(X)$ on the simulated test data.

718 As expected, Deep SHAP values generally increase from the 10th percentile of $g^{XNN}(X)$ to the 90th
719 percentile of $g^{XNN}(X)$, with primarily important global drivers of model behavior contributing to the
720 selected local $g^{XNN}(x^{(i)})$ predictions.

721 Appendix E.2. Discrimination Testing Results

722 Tables A1a and A1b show the results of the disparity tests using the simulated data for two
723 hypothetical sets of class-control groups. Several measures of disparities are shown, with the SMDs
724 calculated using the probabilities from g^{MGBM} and g^{XNN} , false negative rates (FNRs), their ratios, MEs,
725 and AIRs calculated using a binary outcome based on a cutoff of 0.6 (anyone with probabilities of 0.6
726 or greater receives the favorable outcome).¹¹

727 Since g^{MGBM} and g^{XNN} assume that a higher score is favorable (as might be the case if the model
728 were predicting responses to marketing offers), one might consider the relative FNRs as a measure of

729 the class-control disparities. Table A1 shows that protected group 1 has higher relative FNRs under
 730 g^{XNN} (1.13 vs. 1.06). However, in Table A1a the overall FNRs were lower for g^{XNN} (0.357 vs. 0.401).
 731 This illustrates a danger in considering relative class-control metrics in isolation when comparing
 732 across models: despite the g^{MGBM} appearing to be a relatively fairer model, more protected group 1
 733 members experience negative outcomes using g^{MGBM} . This is because FNR accuracy improves for
 734 both the protected group 1 and control group 1, but members of control group 1 benefit more than
 735 those in protected group 1. Of course, the choice of which model is truly fairer is a policy question.

(a) Group size, accuracy, and FNR for g^{MGBM} and g^{XNN} on the simulated test data.

Class	N	Model	Accuracy↑	FNR↓
Protected 1	3,057	g^{MGBM}	0.770	0.401
		g^{XNN}	0.771	0.357
Control 1	16,943	g^{MGBM}	0.739	0.378
		g^{XNN}	0.756	0.314
Protected 2	9,916	g^{MGBM}	0.758	0.331
		g^{XNN}	0.762	0.302
Control 2	10,084	g^{MGBM}	0.729	0.420
		g^{XNN}	0.756	0.332

(b) AIR, ME, SMD, and FNR ratio for g^{MGBM} and g^{XNN} on the simulated test data.

Model	Protected Class	Control Class	AIR↑	ME↓	SMD↓	FNR Ratio↓
g^{MGBM}	1	1	0.752	9.7%	-0.206	1.06
	2	2	1.10	-3.6%	0.106	0.788
g^{XNN}	1	1	0.727	12.0%	-0.274	1.13
	2	2	0.976	1.0%	0.001	0.907

Table A1. Discrimination measures for the simulated test data. Arrows indicate the direction of improvement for each measure.

736 For g^{XNN} , 12.0% fewer control group 1 members receive the favorable offer under the ME column
 737 in Table A1. Of note is that 12.0% is not a meaningful difference without context. If the population
 738 of control group 1 and control group 2 were substantially similar in relevant characteristics, 12.0%
 739 could represent an extremely large difference and would require remediation. But if they represent
 740 substantially different populations, then 12.0% could represent a reasonable deviation from parity. As
 741 an example, if a lending institution that has traditionally focused on high credit quality clients were to
 742 expand into previously under-banked communities, an 12.0% class-control difference in loan approval
 743 rates might be expected because the average credit quality of the new population would be lower
 744 than that of the existing population. Protected group 1's AIR under g^{XNN} is 0.727, below the EEOC
 745 4/5ths rule threshold. It is also highly statistically significant (not shown, but available in resources
 746 discussed in Subsection 1.8). Together these would indicate that there may be evidence of illegal DI.
 747 As with ME and other measures, the reasonableness of this disparity is not clear outside of context.
 748 However, most regulated institutions that do perform discrimination analyses would find an AIR of
 749 this magnitude concerning and warranting further review. Some pertinent remediation strategies for
 750 discovered discrimination are discussed in Subsection 3.3.

751 SMD is used here to measure $g^{MGBM}(X)$ and $g^{MGBM}(X)$ probabilities prior to being transformed
 752 into classifications. (This measurement would be particularly relevant if the probabilities are used in
 753 combination with other models to determine an outcome.) The results show that g^{MGBM} has less DI
 754 than g^{XNN} (-0.206 vs. -0.274), but both are close to Cohen's small effect threshold of -0.20. Whether a
 755 small effect would be a highlighted concern would depend on a organization's chosen threshold for
 756 flagging models for further review.

757 Appendix F. Discrimination Testing and Cutoff Selection

758 The selection of which cutoff to use in production is typically based on the model's use case, rather
 759 than one based solely on the statistical properties of the predictions themselves. For example, a model
 760 developer at a bank might build a credit model where the F1 score is maximized at a delinquency
 761 probability cutoff of 0.15. For purposes of evaluating the quality of the model, she may review
 762 confusion matrix statistics (accuracy, recall, precision, etc.) using cutoffs based on the maximum F1

763 score. But, because of its risk tolerance and other factors, the bank itself might be willing to lend to
764 anyone with a delinquency probability of 0.18 or lower, which would mean that anyone who is scored
765 at 0.18 or lower would receive an offer of credit. Because disparity analyses are concerned with how
766 people are affected by the deployed model, it is essential that any confusion matrix-based metrics of
767 disparity be calculated on the in-production classification decisions, rather than the cutoffs that are not
768 related to what those affected by the model will experience.

769 Appendix G. Recent Fairness Techniques in US Legal and Regulatory Settings

770 Great care must be taken in order to ensure that the appropriate fairness metrics are chosen,
771 because certain metrics may not be appropriate for some use cases. Additionally, the effects of
772 changing the model must be viewed holistically. For example, the mortgage data disparity analysis in
773 Subsection 2.2.3 shows that if one were to choose g^{MGBM} over g^{XNN} because g^{MGBM} has a lower FPR
774 ratio for blacks, it would ultimately lead to a higher FPR for blacks overall, which may represent doing
775 more harm than good.

776 Furthermore, using some recently developed discrimination mitigation methods may lead
777 to non-compliance with anti-discrimination laws and regulations. A fundamental maxim of US
778 anti-discrimination law is that (to slightly paraphrase), “similarly situated people should be treated
779 similarly.”²⁵ A model developed without inclusion of class status (or proxies thereof) considers
780 similarly situated people the same on the dimensions included in the model: people who have the
781 same feature values will have the same model output (though there may be some small or random
782 differences in outcomes due to computational issues). Obviously, the inclusion of protected class status
783 will change model output by class. With possible rare exceptions, this is likely to be viewed with legal
784 and regulatory skepticism today, even if including class status is done with fairness as the goal.²⁶
785 Preprocessing and post-processing techniques may be similarly problematic, because industries that
786 must provide explanations to those who receive unfavorable treatment (e.g., adverse action notices in
787 US financial services) may have to incorporate the class adjustments into their explanations as well.

788 References

- 789 1. Rudin, C. Please Stop Explaining Black Box Models for High Stakes Decisions and Use Interpretable
790 Models Instead. *arXiv preprint arXiv:1811.10154* **2018**. URL: <https://arxiv.org/pdf/1811.10154.pdf>.
- 791 2. Feldman, M.; Friedler, S.A.; Moeller, J.; Scheidegger, C.; Venkatasubramanian, S. Certifying and Removing
792 Disparate Impact. *Proceedings of the 21st ACM SIGKDD International Conference on Knowledge
793 Discovery and Data Mining*. ACM, 2015, pp. 259–268. URL: <https://arxiv.org/pdf/1412.3756.pdf>.
- 794 3. Dwork, C.; Hardt, M.; Pitassi, T.; Reingold, O.; Zemel, R. Fairness Through Awareness. *Proceedings
795 of the 3rd Innovations in Theoretical Computer Science Conference*. ACM, 2012, pp. 214–226. URL:
796 <https://arxiv.org/pdf/1104.3913.pdf>.
- 797 4. Buolamwini, J.; Gebru, T. Gender Shades: Intersectional Accuracy Disparities in Commercial Gender
798 Classification. *Conference on Fairness, Accountability and Transparency*, 2018, pp. 77–91. URL: <http://proceedings.mlr.press/v81/buolamwini18a/buolamwini18a.pdf>.
- 800 5. Barreno, M.; Nelson, B.; Joseph, A.D.; Tygar, J. The Security of Machine Learning. *Machine Learning* **2010**,
81, 121–148. URL: http://people.ischool.berkeley.edu/~tygar/papers/SML/sec_mach_learn_journal.pdf.
- 802 6. Tramèr, F.; Zhang, F.; Juels, A.; Reiter, M.K.; Ristenpart, T. Stealing Machine Learning Models via
803 Prediction APIs. *25th {USENIX} Security Symposium ({USENIX} Security 16)*, 2016, pp. 601–618. URL:
804 https://www.usenix.org/system/files/conference/usenixsecurity16/sec16_paper_tramer.pdf.

25 In the pay discrimination case, *Bazemore vs. Friday*, 478 US 385 (1986), the US Supreme Court found that, “Each week’s paycheck that delivers less to a black than to a similarly situated white is a wrong actionable ...” Beyond the obvious conceptual meaning, what specifically constitutes *similarly situated* is controversial and its interpretation differs by circuit.

26 In a reverse discrimination case, *Ricci v Desafano*, 557 US 557 (2009), the court found that any consideration of race which is not justified by correcting for past proven discrimination is illegal and, moreover, a lack of fairness is not necessarily evidence of illegal discrimination.

- 805 7. Shokri, R.; Stronati, M.; Song, C.; Shmatikov, V. Membership Inference Attacks Against Machine Learning
806 Models. 2017 IEEE Symposium on Security and Privacy (SP). IEEE, 2017, pp. 3–18. URL: <https://arxiv.org/pdf/1610.05820.pdf>.
- 807 8. Shokri, R.; Strobel, M.; Zick, Y. Privacy Risks of Explaining Machine Learning Models. *arXiv preprint*
808 *arXiv:1907.00164* **2019**. URL: <https://arxiv.org/pdf/1907.00164.pdf>.
- 809 9. Williams, M.; others. *Interpretability*; Fast Forward Labs, 2017. URL: <https://www.cloudera.com/products/fast-forward-labs-research.html>.
- 810 10. Friedman, J.H. A Tree-structured Approach to Nonparametric Multiple Regression. In *Smoothing techniques*
811 for curve estimation; Springer, 1979; pp. 5–22. URL: <http://inspirehep.net/record/140963/files/slac-pub-2336.pdf>.
- 812 11. Friedman, J.H.; others. Multivariate Adaptive Regression Splines. *The annals of statistics* **1991**, *19*, 1–67.
813 URL: https://projecteuclid.org/download/pdf_1/euclid-aos/1176347963.
- 814 12. Friedman, J.H. Greedy Function Approximation: a Gradient Boosting Machine. *Annals of statistics* **2001**,
815 pp. 1189–1232. URL: https://projecteuclid.org/download/pdf_1/euclid-aos/1013203451.
- 816 13. Friedman, J.H.; Hastie, T.; Tibshirani, R. *The Elements of Statistical Learning*; Springer: New York, 2001.
817 URL: https://web.stanford.edu/~hastie/ElemStatLearn/printings/ESLII_print12.pdf.
- 818 14. Recht, B.; Re, C.; Wright, S.; Niu, F. HOGWILD: A Lock-free Approach to Parallelizing
819 Stochastic Gradient Descent. Advances in Neural Information Processing Systems (NIPS), 2011,
820 pp. 693–701. URL: <https://papers.nips.cc/paper/4390-hogwild-a-lock-free-approach-to-parallelizing-stochastic-gradient-descent.pdf>.
- 821 15. Hinton, G.E.; Srivastava, N.; Krizhevsky, A.; Sutskever, I.; Salakhutdinov, R.R. Improving Neural Networks
822 by Preventing Co-adaptation of Feature Detectors. *arXiv preprint arXiv:1207.0580* **2012**. URL: <https://arxiv.org/pdf/1207.0580.pdf>.
- 823 16. Sutskever, I.; Martens, J.; Dahl, G.; Hinton, G. On the Importance of Initialization and Momentum
824 in Deep Learning. International Conference on Machine Learning, 2013, pp. 1139–1147. URL: <http://proceedings.mlr.press/v28/sutskever13.pdf>.
- 825 17. Zeiler, M.D. ADADELTA: an Adaptive Learning Rate Method. *arXiv preprint arXiv:1212.5701* **2012**. URL:
826 <https://arxiv.org/pdf/1212.5701.pdf>.
- 827 18. Aïvodji, U.; Arai, H.; Fortineau, O.; Gambs, S.; Hara, S.; Tapp, A. Fairwashing: the Risk of Rationalization.
828 *arXiv preprint arXiv:1901.09749* **2019**. URL: <https://arxiv.org/pdf/1901.09749.pdf>.
- 829 19. Slack, D.; Hilgard, S.; Jia, E.; Singh, S.; Lakkaraju, H. How Can We Fool LIME and SHAP? Adversarial
830 Attacks on Post-hoc Explanation Methods. *arXiv preprint arXiv:1911.02508* **2019**. URL: <https://arxiv.org/pdf/1911.02508.pdf>.
- 831 20. Vaughan, J.; Sudjianto, A.; Brahimi, E.; Chen, J.; Nair, V.N. Explainable Neural Networks Based on Additive
832 Index Models. *arXiv preprint arXiv:1806.01933* **2018**. URL: <https://arxiv.org/pdf/1806.01933.pdf>.
- 833 21. Yang, Z.; Zhang, A.; Sudjianto, A. Enhancing Explainability of Neural Networks Through Architecture
834 Constraints. *arXiv preprint arXiv:1901.03838* **2019**. URL: <https://arxiv.org/pdf/1901.03838.pdf>.
- 835 22. Goldstein, A.; Kapelner, A.; Bleich, J.; Pitkin, E. Peeking Inside the Black Box: Visualizing Statistical
836 Learning with Plots of Individual Conditional Expectation. *Journal of Computational and Graphical Statistics*
837 **2015**, *24*. URL: <https://arxiv.org/pdf/1309.6392.pdf>.
- 838 23. Lundberg, S.M.; Lee, S.I. A Unified Approach to Interpreting Model Predictions. In *Advances in Neural*
839 *Information Processing Systems (NIPS)*; Guyon, I.; Luxburg, U.V.; Bengio, S.; Wallach, H.; Fergus, R.;
840 Vishwanathan, S.; Garnett, R., Eds.; Curran Associates, Inc., 2017; pp. 4765–4774. URL: <http://papers.nips.cc/paper/7062-a-unified-approach-to-interpreting-model-predictions.pdf>.
- 841 24. Lundberg, S.M.; Erion, G.G.; Lee, S.I. Consistent Individualized Feature Attribution for Tree Ensembles.
842 In *Proceedings of the 2017 ICML Workshop on Human Interpretability in Machine Learning (WHI 2017)*; Kim,
843 B.; Malioutov, D.M.; Varshney, K.R.; Weller, A., Eds.; ICML WHI 2017, 2017; pp. 15–21. URL: <https://openreview.net/pdf?id=ByTKSo-m->.
- 844 25. Cohen, J. *Statistical Power Analysis for the Behavioral Sciences*; Lawrence Erlbaum Associates, 1988.
845 URL: <http://www.utstat.toronto.edu/~brunner/oldclass/378f16/readings/CohenPower.pdf>.
- 846 26. Cohen, J. A Power Primer. *Psychological Bulletin* **1992**, *112*, 155. URL: <https://www.ime.usp.br/~abe/lista/pdfn45sGokvRe.pdf>.

- 857 27. Zafar, M.B.; Valera, I.; Gomez Rodriguez, M.; Gummadi, K.P. Fairness Beyond Disparate Treatment &
858 Disparate Impact: Learning Classification Without Disparate Mistreatment. Proceedings of the 26th
859 International Conference on World Wide Web. International World Wide Web Conferences Steering
860 Committee, 2017, pp. 1171–1180. URL: <https://arxiv.org/pdf/1610.08452.pdf>.
- 861 28. Lou, Y.; Caruana, R.; Gehrke, J.; Hooker, G. Accurate Intelligible Models with Pairwise Interactions.
862 Proceedings of the 19th ACM SIGKDD International Conference on Knowledge Discovery and Data
863 Mining. ACM, 2013, pp. 623–631. URL: <http://citeseerx.ist.psu.edu/viewdoc/download?doi=10.1.1.352.7682&rep=rep1&type=pdf>.
- 864 29. Apley, D.W. Visualizing the Effects of Predictor Variables in Black Box Supervised Learning Models. *arXiv preprint arXiv:1612.08468* **2016**. URL: <https://arxiv.org/pdf/1612.08468.pdf>.
- 865 30. Shapley, L.S.; Roth, A.E.; others. *The Shapley value: Essays in Honor of Lloyd S. Shapley*; Cambridge
866 University Press, 1988. URL: <http://www.library.fa.ru/files/Roth2.pdf>.
- 867 31. Hall, P. On the Art and Science of Machine Learning Explanations. KDD '19 XAI Workshop Proceedings,
868 2019. URL: <https://arxiv.org/pdf/1810.02909.pdf>.
- 869 32. Molnar, C. *Interpretable Machine Learning*; christophm.github.io, 2018. URL: <https://christophm.github.io/interpretable-ml-book/>.
- 870 33. Hu, X.; Rudin, C.; Seltzer, M. Optimal Sparse Decision Trees. *arXiv preprint arXiv:1904.12847* **2019**. URL:
871 <https://arxiv.org/pdf/1904.12847.pdf>.
- 872 34. Friedman, J.H.; Popescu, B.E.; others. Predictive Learning Via Rule Ensembles. *The Annals of Applied
873 Statistics* **2008**, 2, 916–954. URL: https://projecteuclid.org/download/pdfview_1/euclid.aoas/1223908046.
- 874 35. Gupta, M.; Cotter, A.; Pfeifer, J.; Voevodski, K.; Canini, K.; Mangylov, A.; Moczydlowski, W.; Van Esbroeck,
875 A. Monotonic Calibrated Interpolated Lookup Tables. *The Journal of Machine Learning Research* **2016**,
876 17, 3790–3836. URL: <http://www.jmlr.org/papers/volume17/15-243/15-243.pdf>.
- 877 36. Chen, C.; Li, O.; Barnett, A.; Su, J.; Rudin, C. This Looks Like That: Deep Learning for Interpretable
878 Image Recognition. Proceedings of Neural Information Processing Systems (NeurIPS), 2019. URL:
879 <https://arxiv.org/pdf/1806.10574.pdf>.
- 880 37. Wilkinson, L. Visualizing Big Data Outliers through Distributed Aggregation. *IEEE Transactions on
881 Visualization & Computer Graphics* **2018**. URL: <https://www.cs.uic.edu/~wilkinson/Publications/outliers.pdf>.
- 882 38. Udell, M.; Horn, C.; Zadeh, R.; Boyd, S.; others. Generalized Low Rank Models. *Foundations and Trends®
883 in Machine Learning* **2016**, 9, 1–118. URL: <https://www.nowpublishers.com/article/Details/MAL-055>.
- 884 39. Holohan, N.; Braghin, S.; Mac Aonghusa, P.; Levacher, K. Diffprivlib: The IBM Differential Privacy Library.
885 *arXiv preprint arXiv:1907.02444* **2019**. URL: <https://arxiv.org/pdf/1907.02444.pdf>.
- 886 40. Ji, Z.; Lipton, Z.C.; Elkan, C. Differential Privacy and Machine Learning: A Survey and Review. *arXiv
887 preprint arXiv:1412.7584* **2014**. URL: <https://arxiv.org/pdf/1412.7584.pdf>.
- 888 41. Papernot, N.; Song, S.; Mironov, I.; Raghunathan, A.; Talwar, K.; Erlingsson, Ú. Scalable Private Learning
889 with PATE. *arXiv preprint arXiv:1802.08908* **2018**. URL: <https://arxiv.org/pdf/1802.08908.pdf>.
- 890 42. Abadi, M.; Chu, A.; Goodfellow, I.; McMahan, H.B.; Mironov, I.; Talwar, K.; Zhang, L. Deep Learning with
891 Differential Privacy. Proceedings of the 2016 ACM SIGSAC Conference on Computer and Communications
892 Security. ACM, 2016, pp. 308–318. URL: <https://arxiv.org/pdf/1607.00133.pdf>.
- 893 43. Wachter, S.; Mittelstadt, B.; Russell, C. Counterfactual Explanations without Opening the Black Box:
894 Automated Decisions and the GDPR. *Harv. JL & Tech.* **2017**, 31, 841. URL: <https://arxiv.org/pdf/1711.00399.pdf>.
- 895 44. Ancona, M.; Ceolini, E.; Oztireli, C.; Gross, M. Towards Better Understanding of Gradient-based Attribution
896 Methods for Deep Neural Networks. 6th International Conference on Learning Representations (ICLR
897 2018), 2018. URL: https://www.research-collection.ethz.ch/bitstream/handle/20.500.11850/249929/Flow_ICLR_2018.pdf.
- 898 45. Wallace, E.; Tuyls, J.; Wang, J.; Subramanian, S.; Gardner, M.; Singh, S. AllenNLP Interpret: A Framework
899 for Explaining Predictions of NLP Models. *arXiv preprint arXiv:1909.09251* **2019**. URL: <https://arxiv.org/pdf/1909.09251.pdf>.
- 900 46. Kamiran, F.; Calders, T. Data Preprocessing Techniques for Classification Without Discrimination.
901 *Knowledge and Information Systems* **2012**, 33, 1–33. URL: <https://bit.ly/2lH95IQ>.

- 909 47. Zhang, B.H.; Lemoine, B.; Mitchell, M. Mitigating Unwanted Biases with Adversarial Learning.
910 Proceedings of the 2018 AAAI/ACM Conference on AI, Ethics, and Society. ACM, 2018, pp. 335–340. URL:
911 <https://arxiv.org/pdf/1801.07593.pdf>.
- 912 48. Zemel, R.; Wu, Y.; Swersky, K.; Pitassi, T.; Dwork, C. Learning Fair Representations. International
913 Conference on Machine Learning, 2013, pp. 325–333. URL: <http://proceedings.mlr.press/v28/zemel13.pdf>.
- 914 49. Kamiran, F.; Karim, A.; Zhang, X. Decision Theory for Discrimination-aware Classification. 2012 IEEE 12th
915 International Conference on Data Mining. IEEE, 2012, pp. 924–929. URL: <http://citeseerx.ist.psu.edu/viewdoc/download?doi=10.1.1.722.3030&rep=rep1&type=pdf>.
- 916 50. Rauber, J.; Brendel, W.; Bethge, M. Foolbox: A Python Toolbox to Benchmark the Robustness of Machine
917 Learning Models. *arXiv preprint arXiv:1707.04131* 2017. URL: <https://arxiv.org/pdf/1707.04131.pdf>.
- 918 51. Papernot, N.; Faghri, F.; Carlini, N.; Goodfellow, I.; Feinman, R.; Kurakin, A.; Xie, C.; Sharma, Y.; Brown,
919 T.; Roy, A.; Matyasko, A.; Behzadan, V.; Hambardzumyan, K.; Zhang, Z.; Juang, Y.L.; Li, Z.; Sheatsley,
920 R.; Garg, A.; Uesato, J.; Gierke, W.; Dong, Y.; Berthelot, D.; Hendricks, P.; Rauber, J.; Long, R. Technical
921 Report on the CleverHans v2.1.0 Adversarial Examples Library. *arXiv preprint arXiv:1610.00768* 2018. URL:
922 <https://arxiv.org/pdf/1610.00768.pdf>.
- 923 52. Amershi, S.; Chickering, M.; Drucker, S.M.; Lee, B.; Simard, P.; Suh, J. Modeltracker: Redesigning
924 Performance Analysis Tools for Machine Learning. Proceedings of the 33rd Annual ACM Conference on
925 Human Factors in Computing Systems. ACM, 2015, pp. 337–346. URL: <https://www.microsoft.com/en-us/research/wp-content/uploads/2016/02/amershi.CHI2015.ModelTracker.pdf>.
- 926 53. Papernot, N. A Marauder’s Map of Security and Privacy in Machine Learning: An overview of current and
927 future research directions for making machine learning secure and private. Proceedings of the 11th ACM
928 Workshop on Artificial Intelligence and Security. ACM, 2018. URL: <https://arxiv.org/pdf/1811.01134.pdf>.
- 929 54. Mitchell, M.; Wu, S.; Zaldivar, A.; Barnes, P.; Vasserman, L.; Hutchinson, B.; Spitzer, E.; Raji, I.D.; Gebru,
930 T. Model Cards for Model Reporting. Proceedings of the Conference on Fairness, Accountability, and
931 Transparency. ACM, 2019, pp. 220–229. URL: <https://arxiv.org/pdf/1810.03993.pdf>.
- 932 55. Bracke, P.; Datta, A.; Jung, C.; Sen, S. Machine Learning Explainability in Finance: an Application to Default
933 Risk Analysis 2019. URL: <https://www.bankofengland.co.uk/-/media/boe/files/working-paper/2019/machine-learning-explainability-in-finance-an-application-to-default-risk-analysis.pdf>.
- 934 56. Friedler, S.A.; Scheidegger, C.; Venkatasubramanian, S.; Choudhary, S.; Hamilton, E.P.; Roth, D. A
935 Comparative Study of Fairness-enhancing Interventions in Machine Learning. Proceedings of the
936 Conference on Fairness, Accountability, and Transparency. ACM, 2019, pp. 329–338. URL: <https://arxiv.org/pdf/1802.04422.pdf>.
- 937 57. Schmidt, N.; Stephens, B. An Introduction to Artificial Intelligence and Solutions to the Problems of
938 Algorithmic Discrimination. *arXiv preprint arXiv:1911.05755* 2019. URL: <https://arxiv.org/pdf/1911.05755.pdf>.
- 939 58. Hoare, C.A.R. The 1980 ACM Turing Award Lecture. *Communications* 1981. URL: <http://www.cs.fsu.edu/~engelen/courses/COP4610/hoare.pdf>.